

First-principles-based simulations of relaxor ferroelectrics

B. P. BURTON*†‡, E. COCKAYNE‡, S. TINTE‡ and
U. V. WAGHMARE§¶

†Institute for Materials Research, Tohoku University, Sendai, 980-8577, Japan

‡Ceramics Division, Materials Science and Engineering Laboratory,
National Institute of Standards and Technology Gaithersburg,
MD 20899-8520, USA

§Theoretical Sciences Unit, Jawaharlal Nehru Center for Advanced Scientific
Research, Jakkur PO, Bangalore 560 064, India

¶International Frontier Center for Advanced Materials, Institute for Materials
Research, Tohoku University, Sendai 980-8577, Japan

(Received 18 October 2005; in final form 25 January 2006)

The phenomenology of $\text{Pb}(\text{B},\text{B}')\text{O}_3$ perovskite-based relaxor ferroelectrics (RFE) is reviewed, with emphasis on the relationship between chemical short-range order and the formation of polar nanoregions in the temperature range between the “freezing” temperature, T_f , and the Burns temperature, T_B . Results are presented for first-principles-based effective Hamiltonian simulations of $\text{Pb}(\text{Sc}_{1/2}\text{Nb}_{1/2})\text{O}_3$ (PSN), and simulations that were done with empirically modified variants of the PSN Hamiltonian. Arbitrarily increasing the magnitudes of local electric fields, caused by an increase in chemical disorder, broadens the dielectric peak, and reduces the ferroelectric (FE) transition temperature; and sufficiently strong local fields suppress the transition. Similar, but more dramatically glassy results are obtained by using the PSN dielectric model with a distribution of local fields that is appropriate for $\text{Pb}(\text{Mg}_{1/3}\text{Nb}_{2/3})\text{O}_3$ (PMN). The results of these simulations, and reviewed experimental data, strongly support the view that within the range $T_f < T < T_B$, polar nanoregions are essentially the same as chemically ordered regions. In PSN a ferroelectric phase transition occurs, but in PMN, a combination of experimental and computational results indicate that pinning from local fields is strong enough to suppress the transition and glassy freezing is observed.

Keywords: First-principles; Relaxor ferroelectrics; PSN; PMN; Perovskite

PACS numbers: 77.80.Bh; 82.35.Jk; 83.10.Rp; 07.05.Tp; 61.43.Bn

1. Introduction

Perovskite-based $\text{Pb}(\text{B}_{1/2}\text{B}'_{1/2})\text{O}_3$ and $\text{Pb}(\text{B}_{1/3}\text{B}'_{2/3})\text{O}_3$ relaxor ferroelectrics (RFE) [1, 2], such as $\text{Pb}(\text{Sc}_{1/2}\text{Nb}_{1/2})\text{O}_3$ (PSN), $\text{Pb}(\text{Sc}_{1/2}\text{Ta}_{1/2})\text{O}_3$ (PST), $\text{Pb}(\text{Mg}_{1/3}\text{Nb}_{2/3})\text{O}_3$ (PMN), $\text{Pb}(\text{Mg}_{1/3}\text{Ta}_{2/3})\text{O}_3$ (PMT), and $\text{Pb}(\text{Zn}_{1/3}\text{Nb}_{2/3})\text{O}_3$ (PZN) are technologically important transducer/actuator materials with extraordinary dielectric and

*Corresponding author. Email: benjamin.burton@nist.gov

electromechanical properties. They also exhibit fundamentally interesting Vogel–Fulcher [3] temperature, T , and frequency, ω , dependence of their dielectric constant, $\epsilon'(T, \omega)$, that is not observed in conventional ferroelectrics (FEs) such as PbTiO_3 or BaTiO_3 , or antiferroelectrics (AFE) such as PbZrO_3 [4]. Uniaxial RFE (e.g. $\text{Sr}_{1-X}\text{Ba}_X\text{Nb}_2\text{O}_6$) were extensively discussed in the review by Kleemann *et al.* [5], but will not be considered here.

In a RFE, $\epsilon'(T, \omega)$ exhibits a broad peak with ω -dispersion over the Hz–GHz range, which clearly indicates relaxation processes at multiple time-scales. The oxymoronic phrase “diffuse phase transition” (DPT) is often used to describe RFE, but there is no phase transition to a RFE state because there is no macroscopic change of symmetry; rather there is a *crossover* between the RFE state and the normal paraelectric (PE) state, which implies that bulk properties asymptotically approach those of the PE state as temperature increases. A distinction should be made between RFEs, and other FE with DPTs, such as $\text{Pb}(\text{Fe}_{1/2}\text{Nb}_{1/2})\text{O}_3$, whose dielectric response does not have Vogel–Fulcher form [6]. Also, one can distinguish between a RFE that freezes to a glassy state, such as PMN, and a system such as PSN, PST, or PZN (see however [7–10]) that exhibits RFE-like ω -dispersion, but also a FE phase transition; for convenience, such systems will be referred to as incipient RFE (iRFE).

In $\text{Pb}(\text{B}, \text{B}')\text{O}_3$ perovskites such as PMN, PSN, and PST, chemical disorder creates local electrostatic fields \vec{h}_i (often called “random” fields [11–13]) which strongly affect their dielectric properties [14–22]. Charged or polar defects, such as Pb vacancies (probably Pb–O divacancies [23]) also contribute to local fields. Chu, Setter and collaborators have shown that an iRFE such as PSN or PST can be transformed to a RFE, by the addition of sufficient vacancies [17–22]. This is particularly significant because it points to average local field strength, $\langle \vec{h}_i \rangle$, as the conjugate field for the RFE order parameter.

Hydrostatic pressure can also be used to reversibly transform an iRFE such as PSN [24] into a RFE without a FE phase transition [24–30]. As discussed below, this should be understood in terms of energetic competition between normal FE ordering, which is pressure sensitive and local fields which are essentially pressure-independent. In ordinary ferroelectrics, e.g. PbTiO_3 or BaTiO_3 , pressure suppresses FE ordering, and at some critical pressure, $P_{\text{FE}} \lesssim 0.2$ GPa, transforms the FE into a PE [31–34].

In $\text{Pb}(\text{B}_{1/3}\text{B}'_{2/3})\text{O}_3$ systems a fully cation-ordered ground-state configuration has never been realized, but long-range 1 : 1 partial order has been demonstrated in PMT [35–38] and short-range order (SRO; ordered regions of approximately 2–6 nm in diameter in a disordered matrix) is observed in PMN [39–46]. Randall and Bhalla [47] concluded from a review of experimental data that inhomogeneities in the SRO are essential for RFE properties to occur. Coupling between \vec{h}_i and FE degrees of freedom leads to the formation of polar nanoregions (PNR) with collective dipole moments [47, 48], and PNR are deemed essential to the ferroglass freezing that is observed in PMN [49]. The relationship between chemical SRO, local fields, and PNR (i.e. coupling between chemical SRO parameters and polarization) is clearly at the root of RFE properties in the $\text{Pb}(\text{B}_{1/2}\text{B}'_{1/2})\text{O}_3$ and $\text{Pb}(\text{B}_{1/3}\text{B}'_{2/3})\text{O}_3$ systems. To clarify the energetics, dynamics, and temperature dependence of coupling between SRO, local fields, and PNR, large-scale molecular dynamics simulations were performed on a first-principles-based effective Hamiltonian model

for PSN, and on empirical modifications of the PSN Hamiltonian that were designed to make it more like a PMN Hamiltonian.

2. Phenomenology

2.1. Burns temperature and below

The maximum temperature for characteristic RFE properties is called the Burns temperature, T_B , above which the system is classically PE. Below T_B , the $PE \rightarrow RFE$ crossover, various physical properties exhibit deviations from those of normal ferroelectrics, as indicated by the following experimental results for PMN: the index of refraction deviates from a Curie–Weiss law [48] (figure 1); the cubic cell volume [50–52] deviates from a linear trend, (figure 2); the intensity of elastic neutron diffuse scattering at $\hbar\omega = 0$, I_{CP} (the “central peak”) increases from zero [52–56] (figure 3); and pair distribution function (PDF) analysis of neutron scattering data [57] exhibits a significant increase in the refined “volume fraction of rhombohedral phase” that optimizes the fit of a two phase, cubic + rhombohedral, model to the data (figure 4).

Burns and Dacol [48] interpreted their refractive index data (figure 1) as indicating the formation of polar clusters “... several unit cells in size...”, that were enhanced in Nb content. The suggestion of compositional heterogeneity as a source for the unusual properties of PMN had already been made by Smolensky [1] and ultimately developed into the space charge model [58], which was subsequently discredited by Akbas and Davies [35–38]. Notwithstanding repeated attempts, no evidence of compositional fluctuations was produced. Rather, it seems clear that the fluctuating quantity is the nonconserved chemical order parameter for 1:1 ordering of the “random site” or “random layer” model proposed by Akbas and Davies [35–38]. In this model, NaCl-type ordering occurs on the B-sites,

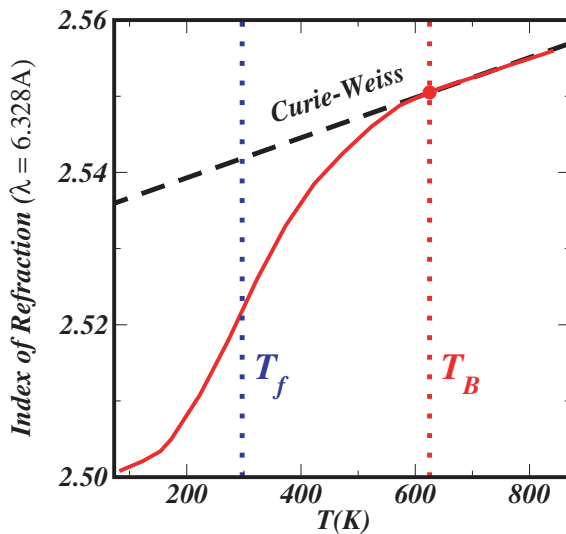


Figure 1. Refractive index as a function of temperature, deviates from a Curie–Weiss law below T_B , after [48].

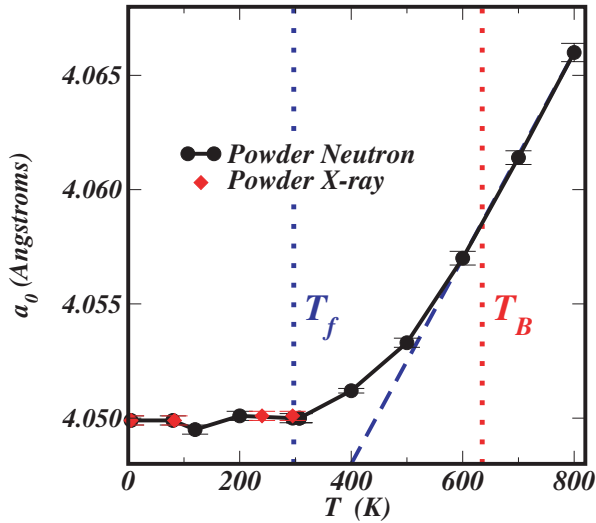


Figure 2. Cubic cell volume as a function of temperature in PMN deviates from linearity below T_B , after [50].

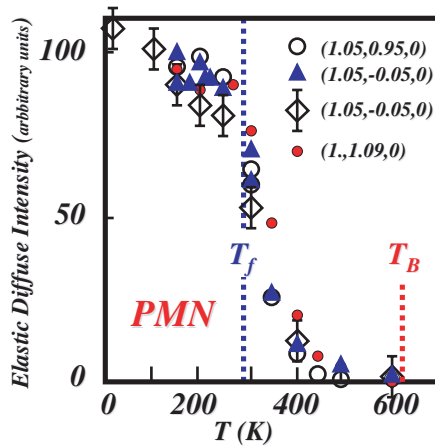


Figure 3. Intensity of the central peak, I_{CP} , as a function of temperature. Below T_B , I_{CP} becomes measurable and in the neighborhood of T_f it rises sharply then plateaus, after [55].

such that B and B' site occupancies are: $B \approx \text{Nb}$; $B' \approx \text{Mg}_{2/3}\text{Nb}_{1/3}$. Note that 1:1 chemical ordering does not imply 1:1 local stoichiometry not even in nanoscale chemically ordered regions (COR).

The “central peak” diffuse scattering results, figure 3, are strongly suggestive of local polar ordering below T_B , as are the Jeong *et al.* PDF analyses, figure 4 [57]. The “central peak” intensity is sensitive to both PNR size and the degree of polar correlation within PNRs, ideally, the PDF analyses [57] should deconvolute these variables. For $T_f < T < T_B$, the striking aspect of the PDF results [57] is that they predict almost no growth of the rhombohedral phase fraction (which Jeong *et al.* [57] equate with PNR) in the interval from T_f to $T = 575 \pm 25$ K. This suggests that

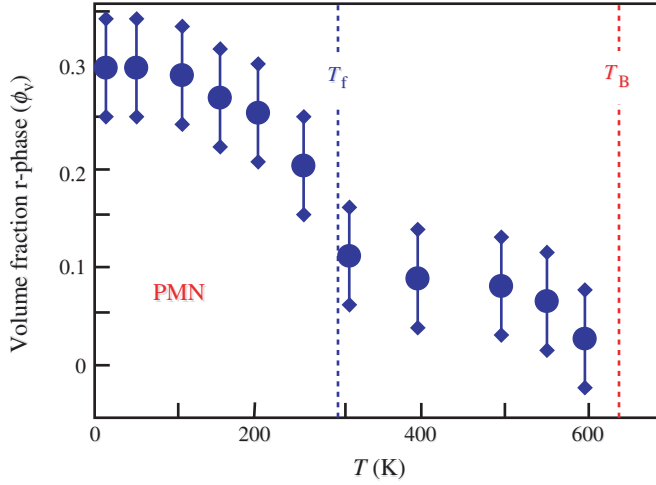


Figure 4. “Volume fraction of rhombohedral phase” (equated with PNR) as a function of temperature, from neutron pair distribution function analysis [57]. In the range $T_f < T < T_B$, $\phi_v \approx \text{constant} \approx 0.1$, and then ϕ_v rises sharply in the neighborhood of T_f , and plateaus at $\phi_v \approx 0.3$, after [57].

as T is reduced from above T_B , the PNR grow briefly in a 35–75 K range just below T_B , but then they do not grow again until T_f is approached.

2.2. Freezing temperature and below

The minimum temperature for RFE-properties is either a point of transition to a FE phase, T_{FE}^* , as in PSN, PST (e.g. Bursill *et al.* [20] and references therein), and PZN [7, 59–61] or a glassy freezing point, T_f , as occurs in PMN [49] (in an applied field [62] PMN transforms to a normal FE with polarization axis [111], $T_{FE} \approx 220$ K). At T_f , PMN exhibits various changes that may be regarded as pre-transition phenomena: fits to powder neutron diffraction data [50], indicate near discontinuous shifts in Pb- and O-positions at ≈ 300 K (figure 5); I_{CP} increases sharply in the neighborhood of T_f [52–56] (figure 3), then plateaus below T_f ; PDF fits to neutron diffraction data exhibit a bifurcation in peak heights, figure 6 at or just above T_f .

The neutron powder diffraction results of Bonneau *et al.* [50] are particularly striking (figure 5). Taken at face value, they appear to indicate discontinuous changes in atomic positions at T_f ; i.e. a first-order phase transition. Macroscopically however, the system remains cubic, and strictly speaking, phase transitions are phenomena that only occur in infinite systems. The natural inference is that *cooperative* atomic displacements occur within regions of the system that are too small to approach the thermodynamic phase transition limit, but are large enough that the cooperativity of their atomic displacements is evident in the powder neutron data. Similar uniform atomic shifts have been reported in PZN [63, 64]. The implied nanotexture is one in which very small domains (volume ≈ 1000 – $10,000$

* T_{FE} is preferred to T_C because the latter implies a critical temperature rather than a first-order transition, and first-order transitions are more common in these systems. Similarly for P_{FE} , the pressure at which an FE \rightarrow PE transition occurs, see below.

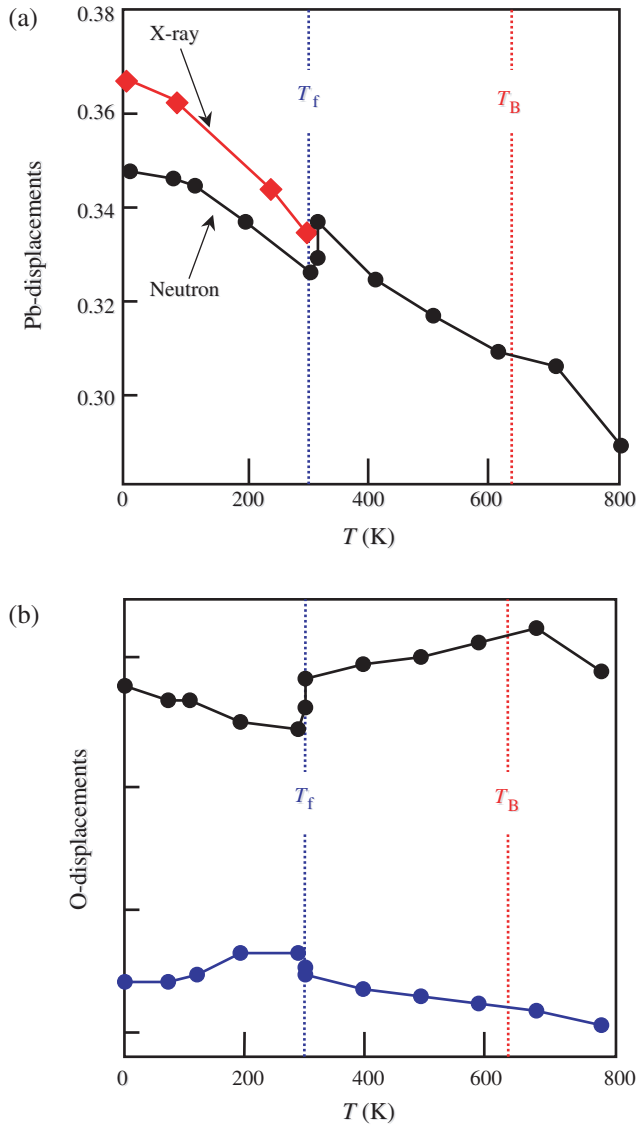


Figure 5. Atomic positions for (a) Pb and (b) O as functions of temperature. The upper curve in (b) is for O-shifts parallel to B–O–B chains, and the lower curve is for O-shifts perpendicular to B–O–B chains, after [50].

unit cells) are sufficiently frustrated with respect to their polar orientation (sufficiently pinned by local fields?) that a phase transition does not occur.

In PMN, the Bonneau *et al.* [50] atomic-shift results (figure 2), the diffuse scattering I_{CP} results [52–56] (figure 3) and the Jeong *et al.* PDF fits [57] (figures 4 and 6) support the conclusion that there is significant PNR growth in the neighborhood of T_f , but no phase transition. Jeong *et al.* [57] interpret their data as indicating that PNR start to grow at $T_f \approx 300$ K, and devote far less attention to the temperature range $T_f < T < T_B$, in which most authors invoke PNR to explain the characteristic RFE properties. In most of this interval, $300 < T < 600$, the Jeong

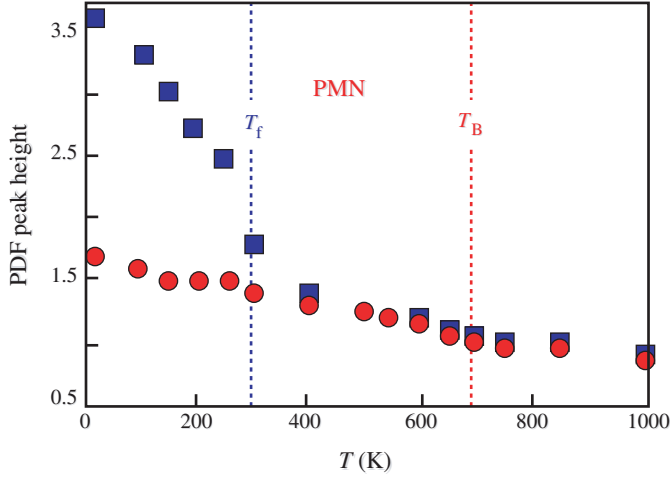


Figure 6. Neutron pair distribution function peak heights that bifurcate at $T \approx T_f$, after [57].

et al. fits suggest a nearly constant volume fraction of rhombohedral phase, $\phi_V \approx 0.1$. Therefore, a more complete interpretation would appear to be that for $T_f < T < T_B$, PNR growth is frustrated, i.e. pinned by local fields, so the PNR do not grow beyond the length scale of the chemically ordered regions. For $T < T_f$, however, PNR growth increases from $\phi_V \approx 0.1 \rightarrow \phi_V \approx 0.3$, where it saturates. In PSN and PZN, FE phase transitions occur, hence one anticipates similar behavior, except that the FE transition preempts freezing.

3. Chemical order–disorder

In $\text{Pb}(\text{B}_{1/2}\text{B}'_{1/2})\text{O}_3$ systems such as PSN and PST, the chemical order–disorder transition is simple to characterize [14, 20, 65–70]. At sufficiently high temperatures ($T > 1723$ K [71]) B-site cations are disordered and at lower T they order into a NaCl type structure. The NaCl configuration is the ground-state for a 1 : 1 mixture of differently charged ions on a simple cubic array of sites, so this result is no surprise [72–75].

In PMN and other $\text{Pb}(\text{B}_{1/3}\text{B}'_{2/3})\text{O}_3$ systems, the situation is not so straightforward. Long-range B-site ordering is not observed in pure PMN at low temperatures, presumably for kinetic reasons. In the structurally analogous $\text{Pb}(\text{Mg}_{1/3}\text{Ta}_{2/3})\text{O}_3$ (PMT), Akbas and Davies [35–38] demonstrated that by adding a small amount of PbZrO_3 , they could achieve “random site” (“random layer”) ordering, which is NaCl-type ordering of B-sites into: $\text{B} \approx \text{Ta}$; $\text{B}' \approx \text{Mg}_{2/3}\text{Ta}_{1/3}$ (presumably Zr^{4+} is about equally distributed on both sites). This structure is not a ground-state, owing to disorder in the (111) layers with $\approx \text{Ta}_{1/3}\text{Mg}_{2/3}$ composition. Inevitably, some ordered configuration of the $\text{Ta}_{1/3}\text{Mg}_{2/3}$ -layer must have lower energy than the disordered configuration. Some candidate ground-state structures based on 30 atom supercells were identified in computational studies [72–77], but more recent work indicates that a 90 atom supercell candidate is still lower in energy [78].

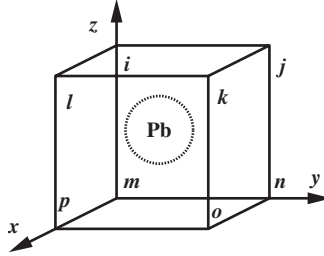


Figure 7. Indexing of B-sites that are nearest neighbors to a Pb atom; Cf. table 1.

Table 1. Local fields at A-sites that have symmetrically distinct nearest neighbor B-site coordination cubes.

Configuration, figure 7 i, j, k, l, m, n, o, p^a	M_{256}^b	$ \bar{h} $ PSN ^c	$ \bar{h} $ PMN	Crystallographic direction
$\bar{1}, \bar{1}, \bar{1}, \bar{1}, \bar{1}, \bar{1}, \bar{1}, \bar{1}$	1	0	0	(0, 0, 0)
$\bar{1}, \bar{1}, \bar{1}, \bar{1}, \bar{1}, \bar{1}, \bar{1}, 1$	8	6.93	10.39	(1, 1, 1)
$\bar{1}, \bar{1}, \bar{1}, \bar{1}, \bar{1}, \bar{1}, 1, 1$	12	11.31	16.97	(1, 1, 0)
$\bar{1}, \bar{1}, \bar{1}, \bar{1}, \bar{1}, 1, \bar{1}, 1$	12	8.00	12.00	(0, 0, 1)
$\bar{1}, 1, \bar{1}, \bar{1}, \bar{1}, \bar{1}, \bar{1}, 1$	4	0	0	(0, 0, 0)
$\bar{1}, \bar{1}, \bar{1}, \bar{1}, \bar{1}, 1, 1, 1$	24	13.27	19.90	(1, 1, 3)
$\bar{1}, 1, 1, 1, \bar{1}, 1, \bar{1}, 1$	8	6.93	10.39	(1, 1, 1)
$\bar{1}, 1, \bar{1}, \bar{1}, \bar{1}, \bar{1}, 1, 1$	24	6.93	10.39	(1, 1, 1)
$\bar{1}, \bar{1}, \bar{1}, \bar{1}, 1, 1, 1, 1$	6	16.00	24.00	(0, 0, 1)
$\bar{1}, 1, \bar{1}, 1, 1, \bar{1}, 1, \bar{1}$	2	0	0	(0, 0, 0)
$\bar{1}, 1, \bar{1}, 1, \bar{1}, 1, \bar{1}, 1$	6	0	0	(0, 0, 0)
$\bar{1}, \bar{1}, 1, 1, \bar{1}, 1, 1, 1$	8	13.86	20.78	(1, 1, 1)
$\bar{1}, 1, \bar{1}, 1, 1, 1, 1, \bar{1}$	24	8.00	12.00	(0, 0, 1)
$1, 1, \bar{1}, \bar{1}, \bar{1}, 1, 1, \bar{1}$	24	11.31	16.97	(1, 1, 0)
$1, \bar{1}, 1, 1, 1, 1, \bar{1}, \bar{1}$	24	6.93	10.39	(1, 1, 1)
$1, 1, \bar{1}, 1, 1, \bar{1}, 1, \bar{1}$	8	6.93	10.39	(1, 1, 1)
$1, 1, 1, 1, 1, \bar{1}, \bar{1}, \bar{1}$	24	13.27	19.90	(1, 1, 3)
$1, \bar{1}, 1, 1, 1, 1, 1, \bar{1}$	4	0	0	(0, 0, 0)
$1, 1, 1, 1, 1, \bar{1}, 1, \bar{1}$	12	8.00	12.00	(0, 0, 1)
$1, 1, 1, 1, 1, 1, \bar{1}, \bar{1}$	12	11.31	16.97	(1, 1, 0)
$1, 1, 1, 1, 1, 1, 1, \bar{1}$	8	6.93	10.39	(1, 1, 1)
$1, 1, 1, 1, 1, 1, 1, 1$	1	0	0	(0, 0, 0)

^aIn column one: $\bar{1}$ implies Sc^{3+} , or Mg^{2+} ; 1 implies Nb^{5+} .

^bMultiplicity (degeneracy) per 256 possible configurations.

^c \bar{h} is normalized such that $\bar{h} = 4\pi\epsilon_0\epsilon|r_{\text{Pb-B}}| \cdot |\bar{E}|$, with ϵ an effective screening parameter.

Even in the absence of local fields from chemical disorder of differently charged ions, e.g. in PbTiO_3 and PbZrO_3 , Pb displaces from ideal perovskite positions to form shorter bonds with a subset of its oxygen nearest neighbors (NN) thereby reducing the total energy. In $\text{Pb}(\text{B}, \text{B}')\text{O}_3$ systems with differently charged B- and B'-ions, Pb *preferentially* displaces towards *underbonded oxygens*, O_u , i.e. O coordinated by two B-site ions with average formal charges less than $4+$ ($\text{Sc}^{3+}\text{-O-Sc}^{3+}$ in PSN or PST; $\text{Mg}^{2+}\text{-O-Mg}^{2+}$ in PMN or PMT) [72–76, 79], figure 8. First-principles studies show that the energies of $\text{Pb}(\text{B}_{1/2}\text{B}'_{1/2})\text{O}_3$ and $\text{Pb}(\text{B}_{1/3}\text{B}'_{2/3})\text{O}_3$ superlattices do not follow the same hierarchy as a purely ionic model, but the energies of the corresponding Ba-based superlattices do. Specifically, the ground states for a purely

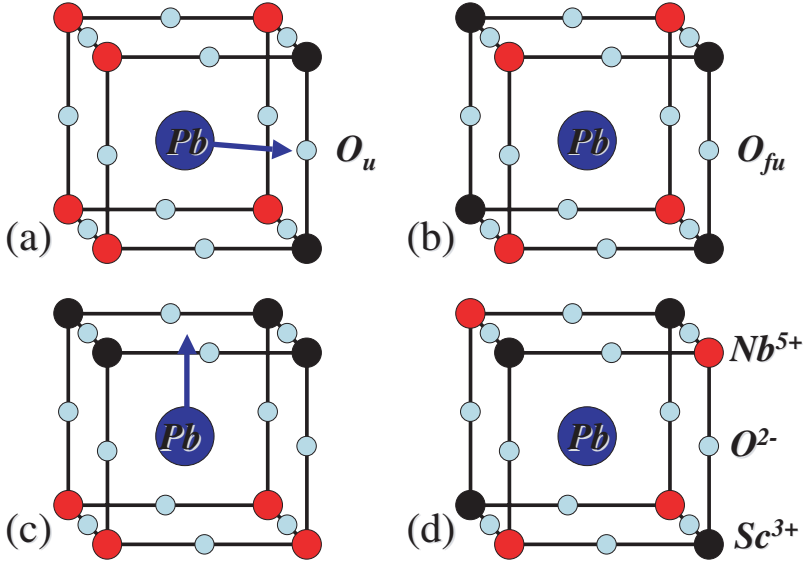


Figure 8. Four of the 22 possible configurations of nearest neighbor B-site ions around a Pb-ion (table 1): (a) \vec{h}_i is in the $[110]$ direction, and the Pb-ion is unstable with respect to displacement towards the underbonded oxygens, O_u , i.e. oxygens between two Sc^{3+} -ions; (b) by symmetry, $\vec{h}_i = 0$, so attraction of the Pb-ion toward the O_{fu} -ions is frustrated, displacing towards one implies a displacement away from the other; (c) \vec{h}_i is in the $[001]$ direction, so the Pb-ion is strongly attracted towards the Sc-layer which has many O_u -ions; (d) by symmetry $\vec{h}_i = 0$, this is the configuration of all Pb-environments in the perfectly ordered PSN ground state.

ionic model are: NaCl-type ordering, as is observed in $Ba(B_{1/2}B'_{1/2})O_3$ systems; and a 1:2 superlattice along $[111]$ (the $[111]_{1:2}$ structure), as is observed in the $Ba(B_{1/3}B'_{2/3})O_3$ systems [e.g. a Mg-layer then two Nb-layers perpendicular to $[111]$ in $Ba(Mg_{1/3}Nb_{2/3})O_3$]. That PMN does not order in $[111]_{1:2}$ fashion indicates the importance of short-range (chemical) effects in the $Pb(B, B')O_3$ systems.

Short-range $Pb^{2+}-O_u$ interactions are also central to the understanding of local fields [80]. Figure 8 shows the connection between the B-site cation distribution around a Pb ion and the local fields in the NN approximation, and the difference between typical large \vec{h}_i and small \vec{h}_i environments. Table 1 is an enumeration of the 22 different NN Pb-environments and their \vec{h}_i values, in normalized units. To first order, it shows the allowed range of local field values that perturb normal polar ordering. In proportion to the difference in the ionic charges between B and B' (Mg^{2+} and Nb^{5+} in PMN, versus Sc^{3+} and Nb^{5+} in PSN), $\langle h_i \rangle_{PMN} = 1.5 \langle h_i \rangle_{PSN}$ in the NN approximation for equivalent nn arrangements of B and B' [80].

Relaxor properties have also been reported in $A(B, B')O_3$ systems with equally charged B and B' ions, e.g. $Ba(Zr_{1-x}Ti_x)O_3$ [81–85]. Here, the source of local fields that are induced by Zr^{4+}/Ti^{4+} chemical disorder must be something more subtle. For example, strain coupling associated with significantly different ionic radii for Zr^{4+} (0.087nm) and Ti^{4+} (0.068 nm) [84]; differences in Zr- and Ti-off-centering in ZrO_6 and TiO_6 octahedra, i.e. fundamental differences between Zr–O and Ti–O bonds; or differences in the *ferroactivities* of Ti and Zr [86]; or coupling between Pb-displacements and the Zr/Ti configuration [86a].

4. PNR size

Assuming that iRFE and RFE systems have PNR below T_B , a fundamental question is, how big they are, and how do PNR length scales vary as functions of T ? Various experimental estimates of PNR size have been published, and they are tabulated in table 2. In 1983, Burns and Dacol [48] suggested that polar clusters in PMN would be "...several unit cells in size..."; Takesue *et al.* [87–89] reported X-ray

Table 2. Reported determinations of PNR length-scales, ℓ_{COR} and/or ℓ_{PNR} , for chemical and/or polar nanoregions in A(B, B')O₃ perovskites.

System	ℓ_{COR} (nm)	ℓ_{PNR} (nm)	Technique	AF ^a	Date [Reference No.]
PSN-D	3 ^b		TEM ^c		1995 [70]
PSN-D	5 ^d		TEM		2001 [15]
PSN-O _{0.4}			XDS ^e	Y	1999 [87, 88]
PSN-O _{1.0}			XDS	Y ^f	1999 [87, 88]
PSN-O			TEM		2001 [15]
PST-D	≈ 2		TEM		1986 [66]
PST-O ₂	40–200 ^g		TEM		1986 [66]
PST-D	10–30		TEM		1995 [70]
PST-O _{0.1}	3.5–5	≈ 3.5–5	TEM		1995 [20]
PST-V _{0.2}	15–50	≈ 5	TEM		1995 [20]
PST-O _{0.93}	100–1000		TEM		1995 [20]
PST-O			TEM	Y ^f	1990 [68]
PSNT-O ^h	60–100		TEM		1995 [70]
PMN	2–6		TEM		1979 [39]
PMN		13.5 at 400 K	NDS		1989 [92]
PMN	2–5		PNPD PDF ⁱ		1994 [43]
PMN			XDS	Y	2000 [93]
PMN		?–30 ^j	XDS	Y	2000 [94]
PMN		3–8 ^k	XDS	Y	2001 [89]
PMN	5	? ^l	XDS		2003 [95]
PMN	< 50		XRD ^m		2003 [49]
PMN		2.5–4.2 ⁿ	NDS ^o		2003 [90]
PMN		0.6–1.2 ^p	NDS		2004 [91]
PMT	2				

^a Antiferroelectric ordering reported.

^b D ⇒ chemically disordered; O ⇒ ordered; V ⇒ Pb vacancies (probably Pb–O divacancy pairs; subscripts on D, O, and V indicate chemical long-range order parameters).

^c TEM = Transmission electron microscopy.

^d Estimated from their figure 6.

^e XDS = X-ray diffuse scattering.

^f $T < 333$ K.

^g COR size increasing with annealing time (2.5–16 h) at 973 K.

^h PSNT = PSN_{0.5}PST_{0.5}.

ⁱ PNPD = Pulsed neutron powder diffraction, PDF = pair distribution function.

^j Below ≈ 173 K PNR > 30 nm freeze out.

^k Decreasing as a function of temperature to 3–4 nm.

^l Decreasing as a function of pressure.

^m XRD = X-ray diffraction.

ⁿ $\ell_{PNR} \approx 3.5, 4.2, 2.5$ nm at $T = 20, 100, 300$ K, respectively.

^o NDS = Neutron diffuse scattering.

^p $\ell_{PNR} \approx 0.6$ and 1.2 nm at $T = 450$ and 225 K, respectively.

diffuse scattering data which indicated "... *approximately spherical correlations with a diameter of 30–40 Å which is most likely the size of polar microregions*"; Blinc *et al.* [49] describe them as "... *smaller than 500 Å...*" an uncertainty-range of ≈ 1.5 orders of magnitude for static values, although most estimates are near the low end of that range. In addition, several estimates indicate temperature dependence in PNR size [57, 89–91].

5. Simulations

5.1. Effective Hamiltonian

Molecular dynamics (MD) simulations were performed using a first principles effective Hamiltonian model [96] H_{eff} for PSN, (the FP-PSN model). H_{eff} for FP-PSN was obtained by adding a local field term to an H_{eff} similar to those previously derived for simple ABO_3 perovskites such as PbTiO_3 and BaTiO_3 [97–100]. In H_{eff} , the full set of atomic displacements from equilibrium positions is projected onto the subspace of low-energy vibrational modes that includes the FE instabilities, represented by local variables $\vec{\xi}_i$ centered on each Pb site i . The polarization in H_{eff} is $(Z^* \sum_i \vec{\xi}_i)/V$, where Z^* is the dipole moment for a unit local distortion.

H_{eff} is obtained from a Taylor expansion of the total energy around a high-symmetry reference structure in terms of $\vec{\xi}_i$, homogeneous strain $e_{\alpha\beta}$, and local fields:

$$H_{\text{eff}} = H(\vec{\xi}_i) + H(e_{\alpha\beta}) + H(\vec{\xi}_i, e_{\alpha\beta}) + H(\vec{\xi}_i, \sigma_l, \nu_{\text{Pb-O}}, \dots). \quad (5.1)$$

The first three terms give a valid H_{eff} for a perovskite without local fields [97–100], (here, the reference structure is a NaCl-ordered PSN cell). $H(\vec{\xi}_i, \sigma_l, \nu_{\text{Pb-O}}, \dots)$ is the local field term [80, 96] in which σ_l indicates contributions from chemical disorder on B-sites, $\nu_{\text{Pb-O}}$ indicates contributions from Pb–O divacancy pairs, and "... " the contribution(s) from any other charged or polar defect(s).

The terms in H_{eff} that determine FE instability are

$$\sum_i \left(A |\vec{\xi}_i|^2 + B |\vec{\xi}_i|^4 + C (\xi_{ix}^4 + \xi_{iy}^4 + \xi_{iz}^4) \right. \\ \left. + D |\vec{\xi}_i|^6 + D' (|\vec{\xi}_i|^2) (\xi_{ix}^4 + \xi_{iy}^4 + \xi_{iz}^4) + D'' (\xi_{ix}^6 + \xi_{iy}^6 + \xi_{iz}^6) + E |\vec{\xi}_i|^8 \right) \quad (5.2)$$

is the Taylor expansion of the local distortion energy. Long-range Coulomb interactions between the dipole moments associated with local distortions are given by

$$\sum_i \sum_{\vec{d}} \frac{(Z^*)^2}{\epsilon_\infty} \cdot \frac{(\vec{\xi}_i \cdot \vec{\xi}_i(\vec{d}) - 3(\vec{\xi}_i \cdot \hat{d})(\vec{\xi}_i(\vec{d}) \cdot \hat{d}))}{|\vec{d}|^3}, \quad (5.3)$$

where ϵ_∞ is the electronic dielectric constant. Short-range corrections to intersite coupling are included out to third neighbors, via the longitudinal and transverse coupling parameters a_L, a_T, c_T . Table 3 lists the numerical values of H_{eff} parameters for the FP-PSN model.

The strain term $H(e_{\alpha\beta})$ is

$$Nf \sum_\alpha e_{\alpha\alpha} + \frac{N}{2} C_{11} \sum_\alpha e_{\alpha\alpha}^2 + \frac{N}{2} C_{12} \sum_{\alpha \neq \beta} e_{\alpha\alpha} e_{\beta\beta} + \frac{N}{4} C_{44} \sum_{\alpha \neq \beta} e_{\alpha\beta}^2,$$

Table 3. Effective Hamiltonian parameters for PSN. Units are eV per five atom cell, except for Z^* , which is in eÅ, and ϵ_∞ , which is dimensionless.

A	-0.8112	a_L	17.24	C_{11}	128.3
B	752.2	a_T	-4.131	C_{12}	38.08
C	542.0	b_L	-0.0340	C_{44}	122.4
D	-1.702×10^4	b_{T1}	-0.0340	g_0	-50.60
D'	6.474×10^4	b_{T2}	1.224	g_1	-136.5
D''	-5.963×10^4	c_L	-0.4300	g_2	-212.6
E	5.708×10^4	c_T	-0.8601	f	1.117
Z^*	25.53	ϵ_∞	7.18	x	-3.041

where C_{11} , C_{12} and C_{44} are the elastic constants and the linear strain parameter f is included to compensate for the error between the simulated room temperature lattice parameter of PSN and the experimental one. The local mode-strain coupling $H(\vec{\xi}_i, e_{\alpha\beta})$ is given by

$$g_0 \left(\sum_{\alpha} e_{\alpha\alpha} \right) \sum_i |\vec{\xi}_i|^2 + g_1 \sum_{\alpha} \left(e_{\alpha\alpha} \sum_i \xi_{i\alpha}^2 \right) + g_2 \sum_{\alpha < \beta} e_{\alpha\beta} \sum_i \xi_{i\alpha} \xi_{i\beta} \quad (5.4)$$

The local field modification to H_{eff} is:

$$-x \sum_i \vec{E}_i \cdot \vec{\xi}_i, \quad (5.5)$$

where \vec{E}_i is the electric field at point i . If the distribution of cations on B-sites is the only source of local fields, then the local electric fields are those obtained from an array of effective point charges of -1 and $+1$ for Sc and Nb, respectively; screened by an effective dielectric constant $\epsilon \sim 10$. The electronic dielectric constant ϵ_∞ is ≈ 7 in PSN; screening by atomic motion not included in H_{eff} accounts for the slightly larger value of ϵ . The value of x in table 3 is for a normalization of \vec{E} such that $|\vec{E}| = 4$ at each Pb-site in a supercell containing alternating Sc and Nb planes in the [001] direction.

5.2. Molecular dynamics and derivative models

Molecular dynamics simulations were performed in $40 \times 40 \times 40$ unit cell simulation boxes; i.e. 64,000 Pb-centered local mode variables that represent 320,000 atoms. For FP-PSN, time averaging is over at least 800 MD snapshots with 100 MD time steps between snapshots (80,000 MD steps ≈ 70 ps). In principle, MD simulations can evaluate $\epsilon'(\omega)$, but accessible time scales on the order of 0.1 ns imply that only frequencies greater than approximately:

$$(0.1 \text{ ns})^{-1} = 10 \text{ GHz} \quad (5.6)$$

are accessible. This allows access to phonon modes, but not to the GHz–Hz frequency range in which $\epsilon'(\omega)$ -dispersion is measured in RFE. Thus, all $\epsilon'(T)$ curves presented below are calculated for the static part of the response, and typical $\epsilon'(\omega, T)$ curves are not reproduced.

In the FP-PSN simulations, experimental microstructures with 1:1 ordered regions of 2–6 nm length scale (PSN [14, 15, 70]; PST [20, 66–70]; PMN [39–46, 58]) are modelled by idealized supercells containing ≈ 4 nm 1:1 chemically

ordered regions (COR) in a percolating disordered matrix (PDM) of chemically disordered regions (CDR).

Simulations allow a complete *spatial* analysis of correlations between chemical- and polar-ordering which has not been achieved experimentally, and therefore an analysis of the characteristic PNR length scale. Because each polar local-mode variable is identified as part of a COR or CDR it is possible to identify which parts of the chemical microstructure have enhanced polarization, or polarization-fluctuations, and to see how the dielectric properties of different chemical domains are correlated with one another. By monitoring cluster–cluster correlations as functions of separation it is possible to distinguish between single- and multi-cluster PNR: multi-cluster PNR will exhibit strong cluster–cluster correlations within the PNR length scale, but not beyond it; with only single-cluster PNR there will be no dependence of cluster–cluster correlations on the separation between the clusters.

Some semiempirical modifications of the FP-PSN model were also simulated. In one modification, the strength of local fields in PSN was arbitrarily increased. In another, a “poor man’s PMN” model (pmPMN) was constructed by combining the FP-PSN dielectric model with a PMN-appropriate \bar{h} distribution. This seems justified, because: (1) PMN and PSN share the same tendency towards [111] directed FE polar ordering, although FE ordering in PMN only occurs in an applied field [62]; (2) from the NN approximation for \bar{h}_i [80], plus the Akbas and Davies results for chemical ordering in PMT and PMN–PSN [35–38, 101] it is possible to construct a realistic \bar{h}_i -distribution for PMN. For pmPMN, the time step was 0.6 fs which implies a 50 ps simulation.

5.3. Previous FP-based simulations

Previous FP-based PSN simulations [96, 102–106] share some common predictions: *Consistent with experiment* (1) a first-order $Pm\bar{3}m \rightleftharpoons R3m$ transition to a FE ground-state in both the chemically ordered and disordered states (experimentally, $R3m$; $a_0 = 4.080 \text{ \AA}$, $\alpha = 89.89^\circ$ at room temperature [113]); (2) some broadening of $\epsilon'(T)$ in the disordered state. *Apparently* contrary to experiment [15], they all predict that the chemically ordered phase in PSN has a higher FE-transition temperature than the chemically disordered phase, $T_{FE}(\text{Ord}) > T_{FE}(\text{Dis})$. This experimental result is surprising because in isostructural $\text{Pb}(\text{Sc}_{1/2}\text{Ta}_{1/2})\text{O}_3$ (PST) the observed order of transitions is $T_{FE}(\text{Ord}) > T_{FE}(\text{Dis})$ [17–22], and one expects the \bar{h}_i that are created by chemical disorder to depress T_{FE} , as in PST. It is possible that oxygen octahedral tilting instabilities (ignored in this work) compete with FE instabilities in a configuration-dependent manner that affects the ordering of the T_{FE} . It is probable, however, that the $T_{FE}(\text{Ord}) < T_{FE}(\text{Dis})$ order in PSN experiments results from a sample preparation problem: long annealing times are required to achieve a high degree of chemical order, and this promotes Pb-loss, which depresses T_{FE} and a more diffuse dielectric peak; e.g. see Perrin *et al.* [15], the “PSN-85” sample in their figure 1(c).

Regarding simulations of $\text{Pb}(\text{Zr}_{1-x}\text{Ti}_x)\text{O}_3$ (PZT), which is not a relaxor but is closely related [107–112].

5.4. Local field configuration in the simulation box

The chemical SRO microstructure maps onto a local field microstructure that perturbs the underlying normal FE behavior of the system. The diffusive chemical

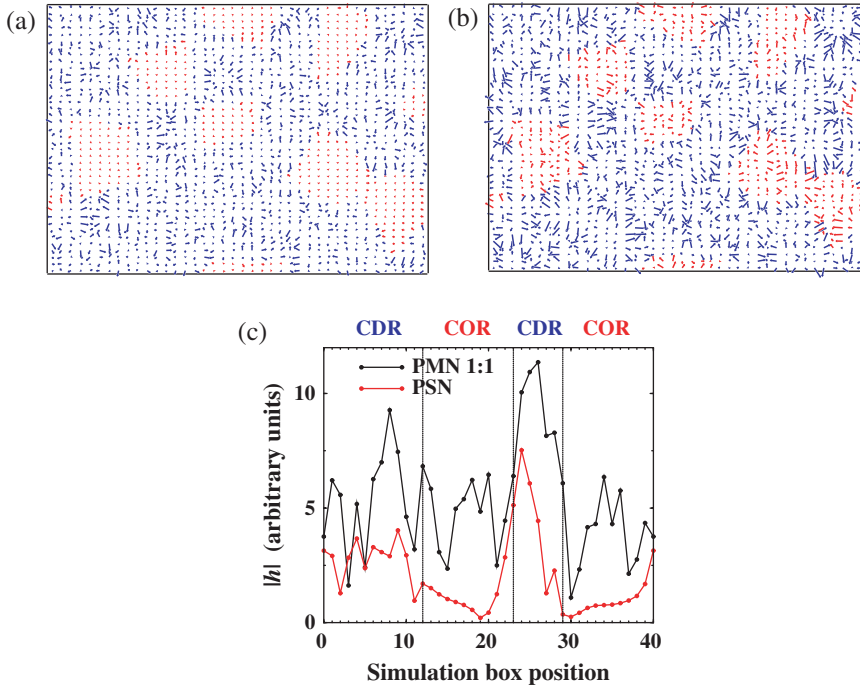


Figure 9. Local fields (arbitrary units) at Pb-sites projected on (110) planes through simulation boxes for: (a) PSN stoichiometry with maximally ordered chemical nanoregions (red) in a random matrix (blue); (b) PMN stoichiometry with 1:1 ordered (but 1:2 stoichiometry) chemical nanoregions in a random matrix; (c) A comparison of one-dimensional lines of Pb-sites through the PSN and PMN simulation boxes in which the y-axis is the absolute value of the local field. In the PSN simulation box, local fields are small in the chemically ordered regions. In the PMN box, they are significant in ordered regions, but larger still in the disordered matrix. PMN local fields in disordered regions are on average ≈ 1.5 times larger than those in PSN because of the greater B-site charge difference (Mg^{2+} and Nb^{5+} in PMN (vs.) Sc^{3+} and Nb^{5+} in PSN).

order–disorder in these systems freezes at temperatures ($T \lesssim 1000$ K) [101] much greater than the temperature range of interest for RFE properties ($T \lesssim 400$ K). Thus, the \vec{h}_i -microstructure corresponding to a given configuration of chemical order may be treated as fixed in the simulated temperature range; i.e. it is sufficient to fix a Sc–Nb configuration and then calculate the local field at each Pb-site once before running the simulation. This procedure implies the approximation of ignoring changes in \vec{h}_i that are caused by inhomogeneous strain.

Quian and Bursill [12] derived a NN approximation (table 1) for \vec{h}_i in PMN and applied it in a two-dimensional Potts-model simulation. A similar three-dimensional model is used here, but the \vec{h}_i (figure 9) are calculated from an electrostatic point-charge model for the full 40^3 B-site configuration in the simulation box. The full box approximation is preferred to a NN approximation because electrostatic interactions are inherently long range, and the NN approximation errs by making $\vec{h}_i = 0$ when $|\vec{h}_i|$ should be small but finite, owing to farther neighbor interactions. The full box approximation errs on the side of over emphasizing distant neighbor interactions that would be screened by intervening charges, but this is not expected to qualitatively change simulation results, whereas it is known that small but finite fields

can have significant qualitative effects on phase transitions. For example, a ferromagnet exhibits no phase transition in an arbitrarily small applied field.

In the simulations presented here, the chemical and therefore local field microstructure of each box consists of 20 COR in a PDM. Each COR contains 800 Pb-sites in a convex, approximately spherical, shape. In order to compare the statistics of the COR and the PDM without artifacts due to averaging over different volumes, the PDM is divided (for accounting purposes only) into 60 CDR of the same size and shape as the 20 COR. The PSN and PMN supercells have the same spatial distributions of COR and CDR, but they differ with respect to bulk composition: 1:1 of $\text{Sc}^{3+}:\text{Nb}^{5+}$ in PSN; 1:2 of $\text{Mg}^{2+}:\text{Nb}^{5+}$ in PMN. Figure 9(a) and (b) shows two-dimensional projections of local fields onto (110) planes through simulation boxes for PSN and PMN. Figure 9(c) is a comparative plot of $|\vec{h}_i|$ values along a single line in the simulation box for the two configurations.

In the PSN box, figure 9(a) and (c), maximally ordered COR are embedded in a PDM. The \vec{h}_i in COR (red) are small and rather homogeneously distributed, while those in the PDM are significantly larger and more variously distributed. If calculations of \vec{h}_i were truncated at the NN approximation, then \vec{h}_i would be exactly zero at many Pb-sites, especially in the COR. Because the COR are maximally ordered, and the PDM is approximated by a random distribution, this microstructure is a limiting case that maximizes the difference in average local field strength, $\Delta\langle|\vec{h}_i|\rangle$, between COR and CDR. Both chemical disorder in the COR and SRO in the CDR would reduce the difference:

$$\Delta\langle|\vec{h}_i|\rangle \equiv \langle|\vec{h}_i|\rangle_{\text{CDR}} - \langle|\vec{h}_i|\rangle_{\text{COR}} \quad (5.7)$$

In the PMN box, figure 9(b) and (c), the COR and CDR both have approximately 1:2 ratio of $\text{Mg}^{2+}:\text{Nb}^{5+}$ stoichiometries but the COR are 1:1 ordered, consistent with the “random site” model of Akbas and Davis [35–38]; i.e. the COR are ordered into alternating (111) layers with compositions Nb and $\text{Mg}_{2/3}\text{Nb}_{1/3}$, respectively. There are two important differences between the local fields in PSN and those in PMN: (1) because of the larger charge-difference Mg^{2+} and Nb^{5+} in PMN, *versus* Sc^{3+} and Nb^{5+} in PSN, $\vec{h}_i(\text{PMN}) \approx 1.5\vec{h}_i(\text{PSN})$ (the factor of 1.5 is exact in the NN approximation, table 1) [80]; (2) in PMN 1:1 random site ordering in the COR reduces the difference between $\langle\vec{h}_i\rangle_{\text{COR}}$ and $\langle\vec{h}_i\rangle_{\text{CDR}}$, relative to the corresponding difference in PSN.

6. Results

6.1. MD simulations of PSN

Figure 10 plots the individual cluster polarizations, $\vec{S}_i(t)$, for the 20 COR and 60 CDR as functions of temperature. Here, subscript $i=O$ indexes a COR, $i=D$ indexes a CDR, and t is the MD time step; \vec{S}_i is used rather than \vec{P}_i to distinguish between individual cluster polarizations and the net polarization for the whole simulation box. Time averaging (represented by triangular brackets $\langle \rangle$ in the equations) is over at least 800 MD snapshots with 100 MD time steps between snapshots (80,000 MD steps \approx 70 ps). At all temperatures, average and maximum values of $\vec{S}_i(t)$, and ε_i , for the COR, are greater than those of the CDR. Thus, COR are regions of enhanced polarization and enhanced polarization fluctuations throughout the T -range sampled in the simulation.

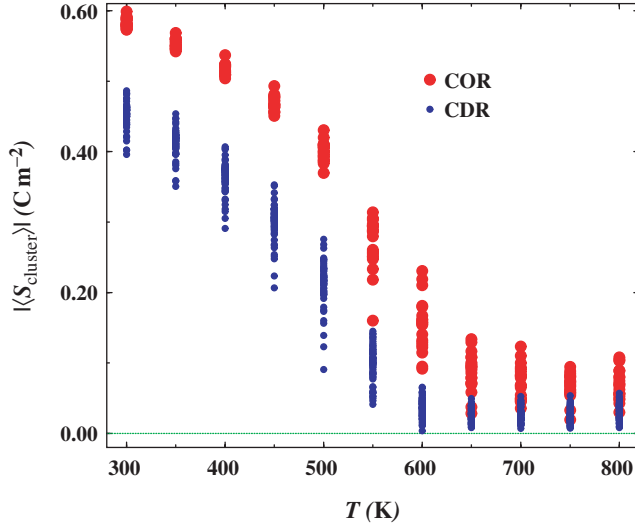


Figure 10. Average polarizations per unit cell for 800 unit cell clusters, as functions of temperature. On average, the chemically ordered regions (COR) have higher polarizations, \bar{S}_i at all temperatures, owing to polarization reductions in the chemically disordered regions (CDR) that are caused by local fields, \vec{h}_i .

Intracluster polarization fluctuations are related to intracluster partial contributions to the total dielectric constant, ε_{ii} :

$$\varepsilon_{ii}(T) \propto \frac{\langle \vec{S}_i(t) \cdot \vec{S}_i(t) \rangle - \langle \vec{S}_i(t) \rangle \langle \vec{S}_i(t) \rangle}{T}. \quad (6.1)$$

Figure 11 shows $\varepsilon_i(T)$. The ε_i are proportional to individual cluster contributions to the the total system dielectric constant. Maxima for $\varepsilon_O(T)$ curves are 2–4 times greater than those for $\varepsilon_D(T)$. The $\varepsilon_O(T)$ -maxima occur over a wider range of temperatures, and the normalized widths of $\varepsilon_O(T)$ -curves are significantly greater than those for $\varepsilon_D(T)$. Thus, cluster polarizations and their fluctuations are significantly greater in COR, which implies that COR must at least act as nuclei for the PNR.

The prediction of a $Pm\bar{3}m \Rightarrow R3m$ FE phase transition is evident in figure 12 which plots T -dependent dot products of cluster moments, $\langle \vec{S}_i(t) \cdot \vec{S}_j(t) \rangle$. These results give the clearest indication that a FE phase transition occurs in the neighborhood of $T = 600$ K. Above 600 K there are about equal numbers of positive and negative values for all three distributions (COR–COD, COR–CDR, CDR–CDR) but below 600 K all three distributions have averages that are greater than zero. All three populations [$\langle \vec{P}_O(t) \cdot \vec{P}_O(t) \rangle$, $\langle \vec{P}_O(t) \cdot \vec{P}_D(t) \rangle$, and $\langle \vec{P}_D(t) \cdot \vec{P}_D(t) \rangle$] have averages greater than zero which indicates a FE-transition throughout the system. Superficially, this contradicts nuclear magnetic resonance studies of a “20–25%” chemically ordered PSN single crystal by Laguta *et al.* [114] which indicate that FE-long-range order is clearly stronger in COR than in CDR, but according to Laguta *et al.* FE-long-range order is only established in the COR. However, Laguta *et al.* also say, “...that even in the disordered parts of the

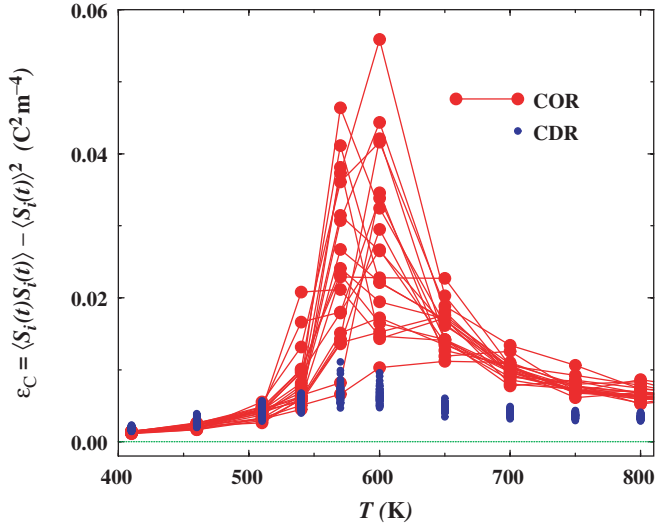


Figure 11. Polarization fluctuations, $\varepsilon_i(T)$, in individual chemically ordered and disordered clusters. Lines connect values for specific ordered clusters, COR. Thus, $\varepsilon_i(T)$ is a cluster dielectric constant, and the dielectric constant for the whole system would be the sum of the 80 ε_i (plus relatively small *intercluster* contributions).

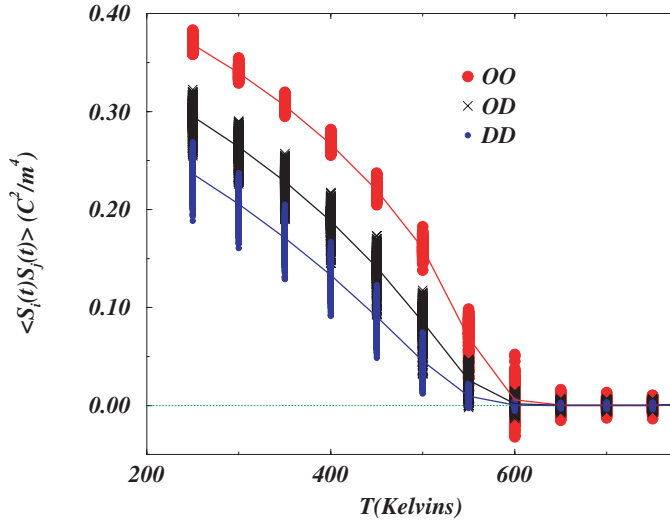


Figure 12. Cluster-polarization dot products as functions of temperature: O–O indicate products between the moments of two chemically ordered clusters, $|\langle \vec{S}_O(t) \cdot \vec{S}_O(t) \rangle|$; O–D for products between chemically ordered and disordered clusters, $|\langle \vec{S}_O(t) \cdot \vec{S}_D(t) \rangle|$; D–D are for two disordered clusters, $|\langle \vec{S}_D(t) \cdot \vec{S}_D(t) \rangle|$. Solid lines link average products. Above $T_{FE} \approx 600$ K, $|\langle \vec{S}_i(t) \cdot \vec{S}_j(t) \rangle| \approx 0$, and below T_{FE} $|\langle \vec{S}_i(t) \cdot \vec{S}_j(t) \rangle| > 0$.

crystal, local polarization acquires a projection along the direction of spontaneous polarization,” which is tantamount to acknowledging FE-long-range order in the CDR as well. Furthermore, Perrin *et al.* [15] report a first-order FE transition in *chemically disordered* PSN. Hence, it appears that the simulations and experiments agree.

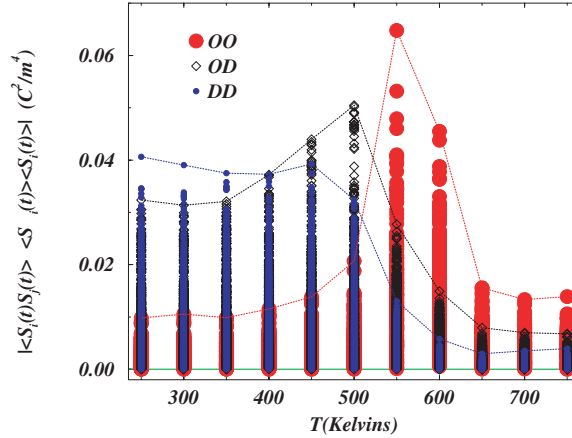


Figure 13. Pairwise cluster–cluster fluctuations as functions of temperature. Without local fields, all pairwise distributions would be identical, and they would all tend to zero as $T \rightarrow 0$. Dotted lines at the maxima of the three distributions are to guide the eye by delineating the different distribution envelopes. The COR–COR fluctuations approximately follow a normal ferroelectric trend, but small local fields in the COR cause a small deviation at low temperature. For the CDR–CDR and CDR–COR fluctuations this deviation is much larger, owing to the much higher average strength of local fields in the CDR. Above T_{FE} , the COR–CDR and CDR–CDR distributions drop significantly below the COR–COR distribution, indicating much stronger COR–COR interactions in this T -range.

The absolute values of pairwise cluster–cluster fluctuations, $|\langle \vec{S}_i(t) \cdot \vec{S}_j(t) \rangle - \langle \vec{S}_i(t) \rangle \langle \vec{S}_j(t) \rangle|$, are plotted in figure 13. Dotted lines connect maxima for each distribution to indicate the envelope of values for each. In a normal FE without local fields, all distributions would be the same and they would all tend to zero as $T \rightarrow 0$. In the simulated nano-ordered configuration, however, pinning by local fields severely hinders alignment of the COR–CDR and CDR–CDR distributions below T_{FE} , so their fluctuations remain large at low T . Below T_{FE} , the COR–COR distribution behaves very much as one would expect it to in a normal FE, except that a small tail persists to low- T . Starting at about 500 K, and persisting above T_{FE} , the COR–CDR and CDR–CDR fluctuations drop rapidly and fall significantly below the COR–COR distribution. Above T_{FE} , the COR–COR distribution remains greater than the COR–CDR and CDR–CDR distributions, which indicates significantly stronger COR–COR interactions in the range $T_{FE} < T < T_B$.

In figure 14, cluster–cluster correlations, $\langle \vec{S}_i(t) \cdot \vec{S}_j(t) \rangle$, are plotted as functions of inter-cluster separations, $d_{i,j}$. If PNR include more than one COR, then one expects significant $d_{i,j}$ -dependence in the COR–COR correlations, particularly in the NN range $d_{i,j} \lesssim 6$ nm. No such trend is evident however (except perhaps for $d_{ij} \lesssim 6$ nm in COR–CDR and CDR–CDR correlations), which strongly suggests that PNR contain no more than a single COR. The apparently random, d_{ij} -independent, distributions of ξ_{OO} , ξ_{OD} , and ξ_{DD} above T_{FE} (figure 14b and c) suggest random-bond type interactions, as postulated in the spherical random bond random field model [115, 116].

It is, of course, conceivable that the PNR are as large as the whole simulation box, but figure 15, which is a snapshot of the local mode polarizations indicates that this is not the case. Arrows in figure 15, indicate the local polarizations at each

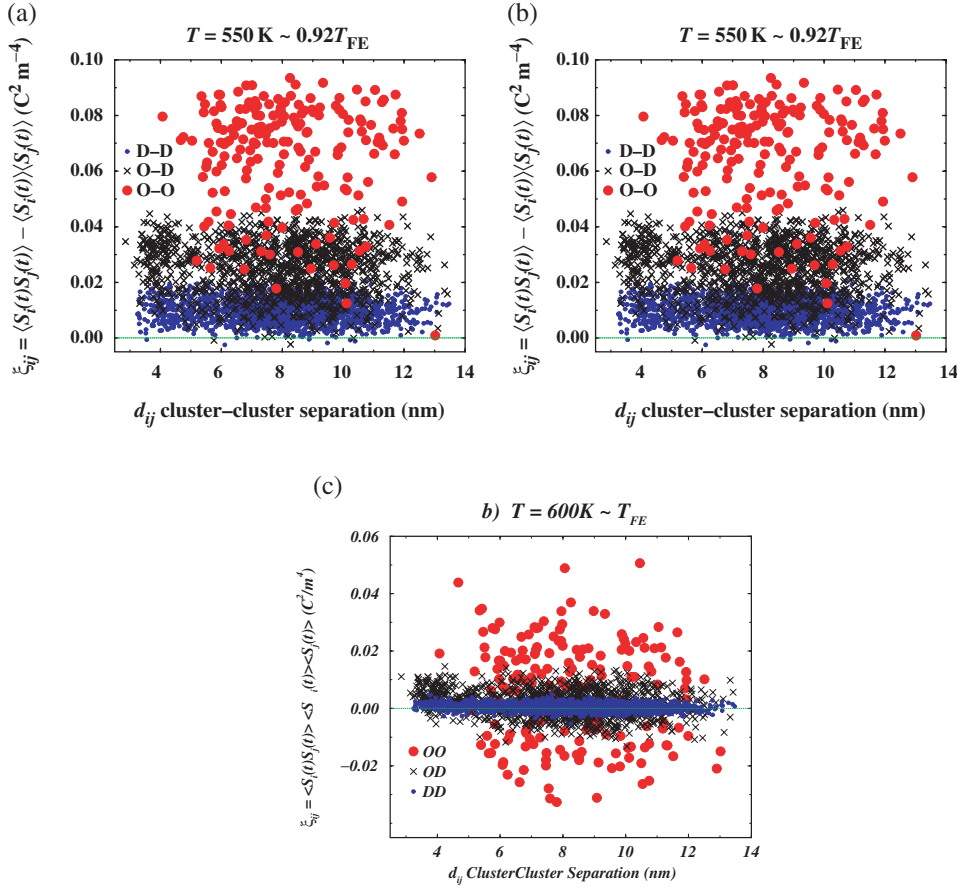


Figure 14. Isothermal pairwise cluster-cluster correlations as functions of inter-cluster separation d_{ij} : (a) $T < T_{\text{FE}}$, 550 K; (b) $T \approx T_{\text{FE}} \approx 600$ K; (c) $T > T_{\text{FE}}$, 650 K. The magnitudes of pairwise correlations exhibit the hierarchy: $|\langle \vec{S}_O(t) \cdot \vec{S}_O(t) \rangle| > |\langle \vec{S}_O(t) \cdot \vec{S}_D(t) \rangle| > |\langle \vec{S}_D(t) \cdot \vec{S}_D(t) \rangle|$. All figures plotted at the same scale. Multi-COR polar nanoregions, PNR, would have strongly correlated near neighbor COR ($d_{ij} \lesssim 6$ nm) and therefore, one would expect some d_{ij} dependence in the COR-COR correlations, but no such trend is evident.

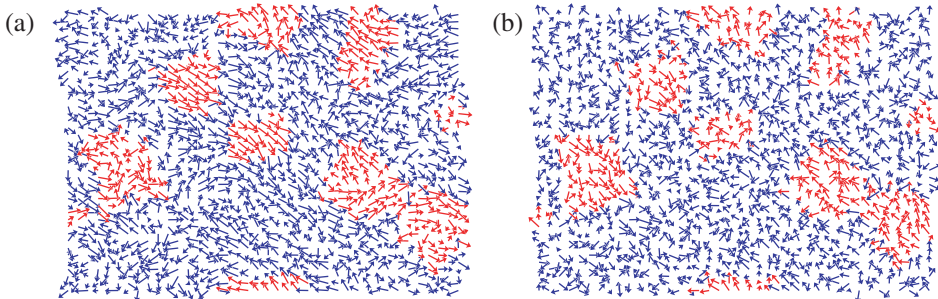


Figure 15. A snapshot of local mode polarizations in: (a) FP-PSN at $T = 600 \text{ K} \approx T_{\text{FE}}$; (b) pmPMN (see below) at $T = 130 \text{ K} \approx T_{\text{max}}$. More highly correlated (red) regions are chemically ordered and the more disordered matrix (blue) is chemically disordered.

Pb-site in a (110) plane through the simulation box. The COR are colored red, and the PDM is blue. Two COR in the upper left quadrant, and along the upper left to lower right diagonal, appear to be highly correlated, but others clearly are not. A movie of 96 such snapshots shows that the COR cluster polarizations rotate relatively freely and independently, while Pb-polarizations in the PDM are less correlated with their near neighbors, and are often restricted in their rotation by local fields.

6.2. Modifications of the FP-PSN model

6.2.1. Pb–O divacancies. The effects of nearest-neighbor Pb–O divacancies on PSN were modeled by fixing the value of the local polar distortion variable, ξ , at randomly selected Pb sites to yield the dipole moment for a Pb–O divacancy in one of the 12 possible [110]-type directions; the specific [110] direction is randomly assigned. The magnitude of the Pb–O dipole moment was set to the value calculated from first principles for PbTiO₃ [23] and the orientations of Pb–O vacancy moments remain fixed throughout the simulation. Figure 16 shows the effect on polarization of adding 1% Pb–O divacancies to the FP-PSN model. The FE phase transition is significantly reduced and the onset of polarization is significantly more gradual, indicating a more glassy system, and possible replacement of the phase transition by a crossover to a RFE.

6.2.1.1. *The effect of increasing $|\vec{h}_i|$.* As noted above, local fields in PMN are a factor of ≈ 1.5 stronger in PMN, than in PSN owing to the larger difference in B-ion charges (rigorously 1.5 in a NN approximation, approximately so in a full box approximation). Thus, the simplest way to modify the FP-based PSN model so that it is more like PMN is to arbitrarily multiply all the $\langle \vec{h}_i \rangle$ by 1.5. Figure 17 shows

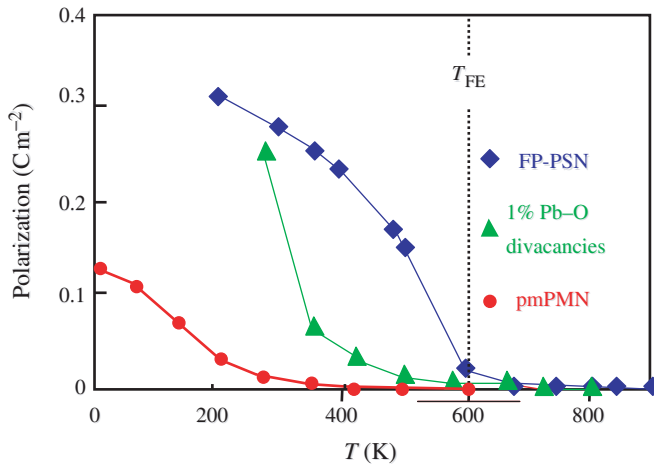


Figure 16. Polarization as a function of temperature for: the FP-PSN model, blue diamonds; the FP-PSN model with 1% Pb–O divacancy pairs, green triangles; and the pmPMN model, red circles. Both the addition of divacancy pairs, and the stronger local fields plus increased chemical disorder in the pmPMN model, significantly reduce T_{FE} . They also cause more gradual onsets of polar ordering, which is characteristic of glassy systems and suggestive of a crossover to a relaxor state.

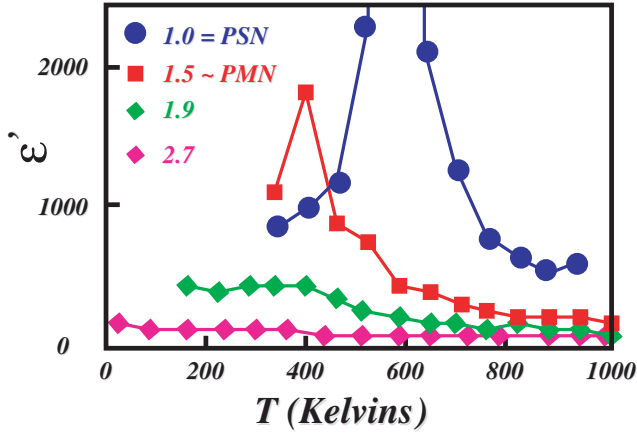


Figure 17. The effect on $\epsilon'(T)$ of arbitrarily increasing $|\bar{h}_i|$: 1.0 labels the FP-PSN curve; 1.5 is approximately the PMN value, which broadens $\epsilon'(T)$ and reduces T_{\max} ; 1.9 may well suppresses the phase transition; 2.7 clearly suppresses it.

the effect on the dielectric constant: the curve labeled with a factor of 1.0 is for the FP-PSN model; a factor of 1.5 increase broadens $\epsilon'(T)$, and reduces T_{FE} as one expects in an iRFE or RFE; a factor 1.9 increase severely broadens $\epsilon'(T)$, and may well suppress the phase transition; a factor of 2.7 is clearly sufficient to suppress the phase transition.

6.2.1.2. *Poor Man's PMN*. Figure 15(b), 16, 18, 19 and 20 plot results of the pmPMN model which combines the FP-PSN dielectric model with a PMN-appropriate distribution of local fields. Figure 15(b) is a polarization snapshot at $T = 130 \text{ K} \approx T_{\max}$ which highlights the greater polar disorder in the pmPMN model relative to the FP-PSN model. Figure 16 plots polarization as a function of temperature. Polar ordering is predicted at $T \lesssim 400\text{--}500 \text{ K}$, but the $P(T)$ curve does not behave as one would expect for a critical, much less first-order, transition. Rather, $P(T)$ gives the impression of approaching zero asymptotically as T increases. This is similar to what is predicted for the addition of Pb–O divacancies, figure 16. It is also similar to the $P(T)$ -curve labeled “Disordered(2)” in figure 8 of Setter and Cross [65]; a chemically disordered PST sample that has a RFE-like $\epsilon'(T)$ -curve, and that was later found to have significant Pb vacancies. Thus, the $P(T)$ -curve for pmPMN is strongly suggestive of a crossover to a RFE, rather than a critical- or first-order FE-phase transition.

Calculated $\epsilon'(T/T_{\max})$ and $\epsilon'(T - T_{\max})$ curves for chemically ordered PSN (FP-PSN₀, in which all $h_i = 0$), and for the FP-PSN and pmPMN models are plotted in figure 18(a) and (b) respectively. Surprisingly, relative to the FP-PSN₀ simulation, the FP-PSN model exhibits very little broadening in either relative or absolute units. However, the pmPMN model exhibits dramatic $\epsilon'(T/T_{\max})$ broadening, and some $\epsilon'(T - T_{\max})$ broadening as well, which is strongly suggestive of iRFE or RFE character in the pmPMN model.

Figure 19 plots pairwise cluster polarization dot products which were used to establish the FE-phase transition in FP-PSN. For pmPMN, they clearly indicate much more pretransition short- to medium-range polar ordering, and average values

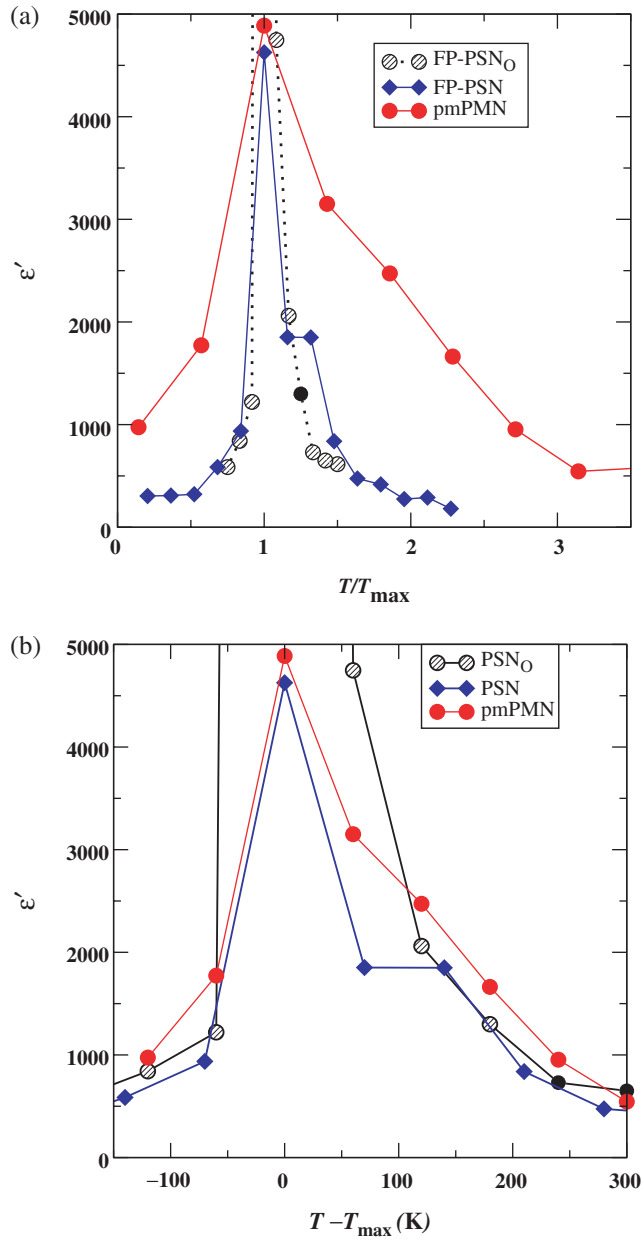


Figure 18. Comparison of pmPMN- and FP-PSN model predictions for dielectric constants as functions of (a) reduced temperature, T/T_{\max} , and (b) $T - T_{\max}$. Relative to chemically ordered PSN, FP-PSN_O, the FP-PSN model exhibits little or no broadening, but pmPMN peak is dramatically broadened in (a) and significantly so in (b). Here, T_{\max} is the temperature at which a maximum value of ϵ' was calculated, and it probably does not correspond to the value one would obtain with smaller T -intervals between simulations.

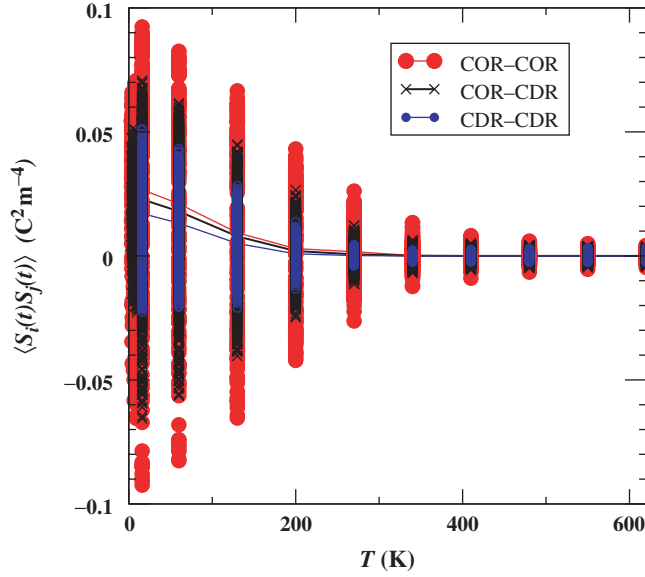


Figure 19. Cluster polarization dot products for the pmPMN model; cf. figure 12. It is not clear if a phase transition occurs or not, but pretransition short-range polar ordering is significantly enhanced relative to the FP-PSN model.

clearly become positive definite below about 200 K, recall that these are essentially the square of the Edwards Anderson order parameter, not long-range order parameters. The polarization which is a long-range order parameter does depart from zero at $T \approx 500$ K, figure 16, but as noted earlier it does so very gradually. This may be a finite size limitation in the pmPMN simulation; i.e. with such high a value of $\langle h_i \rangle$, the 40^3 unit cell system may be small enough to show significant finite-size effects that are not apparent at the lower values of $\langle h_i \rangle$ which characterize FP-PSN. Thus, one clearly demonstrates a phase transition in FP-PSN but the results for pmPMN are less well defined.

The strongest prediction of RFE behavior in the pmPMN model is evident in figure 20, where $\varepsilon_i(T)$ is plotted for the 20 COR and 60 CDR. The way in which $\varepsilon_i(T)$ for the COR dominate the susceptibility in the temperature range $200 \text{ K} < T < 600 \text{ K}$, clearly indicates that they are acting as nanoscale regions of enhanced polarizability, i.e. PNR. It also indicates that broadening of the $\varepsilon'(T/T_{\max})$ curve at $T/T_{\max} \gtrsim 1.5$, is primarily caused by higher- T contributions from the COR.

If one interprets the 200 K departure from zero of average COR-COR, COR-CDR and CDR-CDR fluctuation values as T_{FE} or T_f , then it is natural to estimate $T_B \approx 400\text{--}500$ K.

7. Discussion

7.1. Simulation results

The simulations do not reproduce $\varepsilon'(\omega)$ -dispersion because that requires excessively long MD runs to access the appropriate Hz-GHz frequency range. They do however,

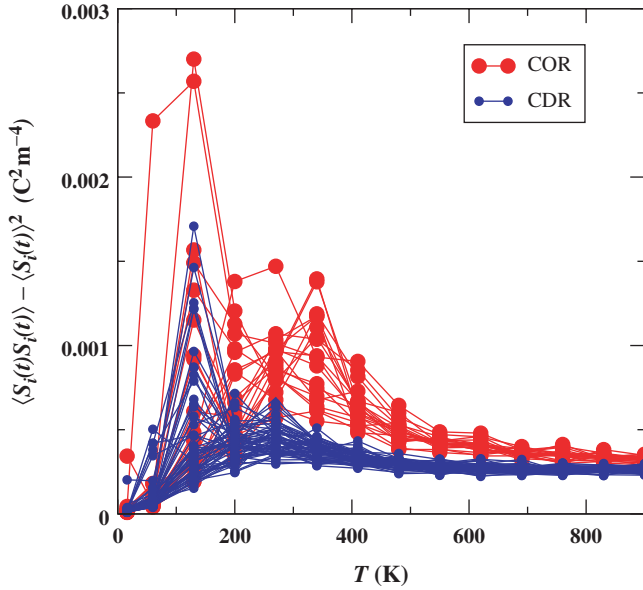


Figure 20. Polarization fluctuations, $\varepsilon_i(T)$, in individual COR and CDR for the pmPMN model; lines connect values for specific clusters. Clearly, the COR dominate the susceptibility in the temperature range $200 \text{ K} < T < 600 \text{ K}$, presumably T_{FE} or $T_f < T < T_B$; cf. figure 11.

reproduce $\epsilon'(T/T_{\max})$ -broadening and suppression of the FE phase transition in response to a sufficient increase in $|\langle \bar{h}_i \rangle|$. This result obtains regardless of how $|\langle \bar{h}_i \rangle|$ is increased: by arbitrary enhancement of the $\langle \bar{h}_i \rangle$, figure 17; by addition of Pb–O divacancy pairs, figure 16; or by increased chemical disorder and a greater difference in B-site ion charges, as in the pmPMN model, figures 15(b), 16, 18–20.

Both the FP-PSN and pmPMN models predict a hierarchy of cluster–cluster correlations:

$$|\xi_{OO'}| > |\xi_{OD}| > |\xi_{DD'}| \quad (7.1)$$

which implies the spatial mapping $\text{COR} \approx \text{PNR}$ above T_{FE} , or presumably, T_f . At $T_{FE} < T < T_B$, all the strong correlations are COR–COR, but they are not so strong as to imply multi-COR PNR, or there would be d_{ij} dependence in the COR–COR correlations, particularly at NN COR–COR distances, $d_{ij} \lesssim 6 \text{ nm}$. A simulation value for T_B , was not determined, but experimentally [15], $T_B \approx 1.1 T_{FE}$ for PSN, consistent with enhanced simulation values for $\varepsilon_O(T)$ above T_{FE} ; i.e. $1.1 T_{FE}$ is approximately the temperature at which dispersion becomes evident in the experimental data [15], and it is approximately where one starts to see substantial nonlinear enhancement of the difference between $\varepsilon_O(T)$ and $\varepsilon_D(T)$ in figure 13. To summarize:

- COR are nanoscale regions of the system [39, 43–46] that have enhanced polarization at all T , figure 10.
- COR polarization fluctuations are also enhanced, figures 11 and 20, owing to their low concentrations of local fields. Local fields in the CDR hinder cooperative polarization rotations in the PDM, while the reduced

concentration of local fields in the COR allow cooperative rotations (uniform shifts?) of greater numbers of NN ions.

- The absence of cluster–cluster separation dependence in COR–COR correlations, figure 14, indicates the absence of multi-COR PNR above T_{FE} .

Thus, *the characteristic length scale for chemical SRO is predicted to be the same as that for the PNR in the range $T_{FE} < T < T_B$* , provided one is content to consider PNR as nanoscale regions of enhanced polarization, and enhanced polar fluctuations, in a less polarized and less susceptible matrix. In PMN, the prediction $COR \approx PNR$, for $T_f < T < 575 \pm 25 \text{ K} < T_B$, is strongly supported by the powder neutron PDF results of Jeong *et al.* [57], figure 4. For PMN, they report an essentially constant rhombohedral (interpreted as PNR) phase fraction, $\phi_V \approx 0.1$, for $T_f \approx 300 \text{ K} < T < 575 \pm 25 \text{ K}$, which indicates that PNR are not growing in this T -range. This is exactly what one expects if the PNR length-scale is pinned by the chemical SRO.

The prediction that $COR \approx PNR$ also suggests a plausible explanation for the observed uniform shift in atomic displacements near T_f in PMN [50, 54]: COR act as nuclei for PNR growth above T_f ; at $T \approx T_f$, PNR polar orientations become fixed and PNR grow, which implies that atomic shifts propagate from the COR out into the PDM; local fields pin the polar orientations of these PNR haloes sufficiently to prevent reorientation; glassy freezing occurs when the expanded PNR COR with mutually aligned PDM haloes, impinge on their neighbors.

7.2. Pressure

Hydrostatic pressure strongly influences normal FE transitions [31–34], as well as RFE properties [5, 24–30]. In general, increasing pressure depresses T_{FE} , and sufficient pressure yields a $FE \rightarrow PE$ transition. First-principles calculations, e.g. [117–119] indicate that the depths of normal FE potential wells are strongly volume-dependent, and that for systems such as $PbTiO_3$, $BaTiO_3$, and $Pb(Ti_{1/2}, Zr_{1/2})O_3$ -supercells, an increase in pressure destabilizes the FE-phase by reducing the well depth of the FE distortion.

In PMN [26–28] which exhibits no FE-transition in the presence of an applied field, an increase in pressure enhances the RFE character [5]. In iRFE systems such as $PZN_{0.985}PT_{0.015}$ [26] and PSN [24] pressure induces a RFE state. Something of an exception is $Pb(In_{1/2}Nb_{1/2})O_3$ (PIN) which is AFE when chemically ordered, but a RFE when sufficiently disordered. In a sample with intermediate chemical order (LRO parameter = 0.4) an $RFE \rightarrow AFE$ transition can be induced by application of 0.4 GPa [120–122]. Samara and coworkers [5, 26, 28] discuss the dominant trend, excluding PIN, in terms of pressure reducing PNR correlation lengths, i.e. PNR size, but to the extent that PNR correlation lengths are fixed by chemical SRO, this description oversimplifies. As discussed above in connection with uniform atomic shifts, growth of PNR haloes beyond the COR and into the PDM is likely to be the relevant correlation length near T_{FE} or T_f . Pressure reduces the driving force for normal FE ordering in the system as a whole. Thus, increased pressure reduces the propagation of polar order into the PDM and from one COR to its neighbors. The stronger the driving force, the easier it is for polar order to propagate throughout the system via a phase transition. The weaker the driving force, the more the system behaves like a collection of disconnected polar regions in a less polar matrix.

That pressure acts to reduce the driving force for normal FE ordering, in the model Hamiltonians is evident from the negative signs of the g_0 and g_1 coupling terms in H_{eff} [123]. Increased pressure results in a *relative* increase in the $H(\vec{\xi}_i, \sigma_i, \nu_{\text{Pb-O}}, \dots)$ term, which is pressure-independent to the first order*, i.e. in $\langle \vec{h}_i \rangle$, by reducing the competition from normal FE-ordering, through the local mode-strain coupling term $H(\vec{\xi}_i, e_{\alpha\beta})$. Pressure acts as if it was a conjugate field for the RFE order parameter, via *relative enhancement* of $H(\vec{\xi}_i, \sigma_i, \nu_{\text{Pb-O}}, \dots)$, which happens because $H(\vec{\xi}_i, e_{\alpha\beta})$ is reduced.

Pressure can be explicitly included in the H_{eff} by adding a pV term, assuming that the variables which define H_{eff} at zero pressure also define it at elevated pressure. Preliminary results for the FP-PSN model indicate that T_{FE} decreases with increasing pressure, as expected, and that an FE \rightarrow PE transition occurs at sufficiently high pressure, P_{FE} . Elevated pressure simulations predict $T_{\text{FE}}(\text{ORD}) > T_{\text{FE}}(\text{DIS})$, as in the zero pressure simulations. Quantitatively however, predicted values of P_{FE} are as much as an order of magnitude larger than experimental values [24].

7.3. Pb-vacancies and $\langle \vec{h}_i \rangle$ as a conjugate field of q_{EA}

The work of Chu, Setter and others on Pb-vacancies in the iRFE systems, PSN and PST [17–22], is particularly significant because it implicitly identifies $\langle \vec{h}_i \rangle$ as the pseudoconjugate field for the RFE order parameter; “pseudoconjugate” because $\langle \vec{h}_i \rangle$ is inhomogeneous with respect to chemical SRO at the same length scale that PMN polar ordering occurs, and because RFE \rightleftharpoons PE is a crossover rather than a phase transition. In PSN and PST, iRFE \rightarrow RFE transitions are induced by adding sufficient Pb-vacancies, and thereby increasing $\langle \vec{h}_i \rangle$. Although these experiments were not explicitly reversed (RFE \rightarrow iRFE via removal of vacancies) there is no reason in principle that this could not be done. As demonstrated in the simulation results, increasing $\langle \vec{h}_i \rangle$ by arbitrarily increasing \vec{h}_i , figure 17, or by creating more chemical disorder (as in the pmPMN model), or by including Pb–O divacancies, figure 16, yields the same effects on T_{FE} and $\epsilon'(T)$; T_{FE} is depressed and $\epsilon'(T/T_{\text{max}})$ is broadened when $\langle \vec{h}_i \rangle$ is increased (FP-PSN \rightarrow pmPMN) and at sufficiently large $\langle \vec{h}_i \rangle$, the FE-transition and the dielectric peak are suppressed.

In a normal FE, the order parameter is polarization, \vec{P} , and its conjugate field is the electric field, \vec{E} . In a RFE, the Edwards Anderson order parameter, $q_{\text{EA}} = |\langle S_i \cdot S_j \rangle|^{1/2}$ [5, 96, 124], replaces polarization and the average local field, $\langle \vec{h}_i \rangle$, is conjugate. The Edwards Anderson order parameter is closely related to the spin products plotted in figure 12. Figure 21 is a schematic diagram in which $\langle \vec{h}_i \rangle$ and pressure are plotted as pseudoconjugate fields for the RFE order parameter. Above some minimum value of $\langle \vec{h}_i \rangle$, the FE phase transforms into the RFE portion of the PE phase, which crosses over into the normal PE state in the neighborhood of T_{B} . Below the minimum value of $\langle \vec{h}_i \rangle$, a normal FE \rightarrow PE transition occurs. If the RFE order parameter had spherical symmetry, then according to Imry and Ma [125] the minimum value would be zero.

*Reducing the volume increases $\langle \vec{h}_i \rangle$ slightly by reducing the separations between Pb- and B-site ions, but this increase is small compared to the strain-coupling effect; less than 5% at 20 GPa.

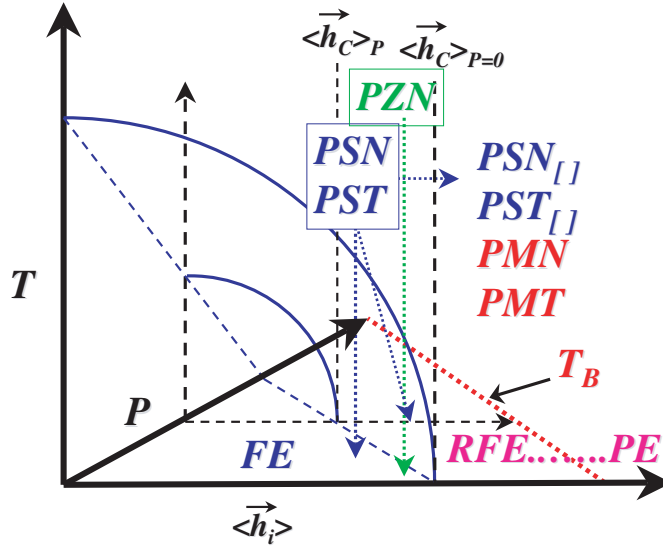


Figure 21. Schematic representation of the similarities and differences between various $\text{Pb}(\text{B},\text{B}')\text{O}_3$ systems that exhibit iRFE or RFE properties. The suggestion is that the essential difference between PMN and PSN is the higher density of stronger local fields in PMN, i.e. larger $\langle \vec{h}_i \rangle$. PSN, PST, and PZN exhibit ferroelectric transitions can be transformed into RFEs by increasing local fields with the addition of Pb–O divacancy pairs (subscript [] indicates vacancies), or by increasing hydrostatic pressure.

7.4. PMN versus PZN

An interesting question is why PMN exhibits glassy freezing, but PZN exhibits a FE phase transition. To first order, the \vec{h}_i in iRFE PZN are equal to those in RFE PMN, which suggests that iRFE PZN is very close to full RFE character, and RFE PMN is very close to having a FE phase transition. The difference in ionic radii (effective pressure) between VI coordinated Zn^{2+} (0.074 nm) and Mg^{2+} (0.072 nm) [126], is so small that it seems an unlikely source of explanation. A further complication is that beneath a $\approx 10\text{--}50\ \mu\text{m}$ rhombohedral skin [7–10], PZN single crystals appear to be cubic at low T , like PMN.

8. Conclusions

In the simulations, depression of T_{FE} , broadening of $\epsilon'(T/T_{\text{max}})$ and enhanced COR–COR correlations and polar fluctuations above T_{FE} , are all strongly suggestive of RFE properties. In the temperature interval $T_{\text{FE}} < T < T_{\text{B}}$, or $T_f < T < T_{\text{B}}$, the length scales of COR and PNR are essentially the same because intracluster COR fluctuations and COR–COR correlations coincide with enhanced polarization fluctuations and pairwise correlations, and also because the PNR do not grow, as T decreases, until T_{FE} or T_f is approached. This explains why Jeong *et al.* [57] get $\phi(T) \approx 0.1 \approx \text{constant}$ for PMN in the interval $T_f < T < 575 \pm 25\ \text{K}$; PNR growth is pinned by local fields such that $\text{COR} \approx \text{PNR}$.

Average local field strength $\langle \vec{h}_i \rangle$ is the pseudoconjugate field for the RFE order parameter, q_{EA} , and it is essentially independent of hydrostatic pressure. Hydrostatic pressure, as pointed out by Samara [32], is a much “cleaner” variable: it reduces the driving force for normal FE ordering, which tilts the $FE \rightleftharpoons RFE$ competition in favor of the RFE.

Acknowledgements

B.P.B thanks the Kawazoe Laboratory of the Institute for Materials Research, Tohoku University, Sendai, Japan; most of this article was written by BPB while he was a visiting professor in the Kawazoe Laboratory. U.V.W thanks the Central Computing Facility of JNCASR, funded by the Department of Science and Technology, Government of India.

References

- [1] G.A. Smolensky, A.I. Agranovskaya, *Sov. Phys. Sol. State* **1** 1429 (1959).
- [2] L.E. Cross, *Ferroelectrics* **76** 241 (1987).
- [3] D. Viehland, S.J. Jang, L.E. Cross and M. Wuttig, *J. Appl. Phys.* **68** 2916 (1990).
- [4] M.E. Lines and A.M. Glass, *Principles and Applications of Ferroelectrics and Related Materials* (Clarendon Press, Oxford, 1979).
- [5] W. Kleemann, G.A. Samara and J. Dec, in *Polar Oxides: Properties, Characterization, and Imaging*, edited by R. Waser, U. Bottger and S. Tiedke (WILEY-VCH Verlag, GmbH & Co. KGaA, Weinheim, 2005), p. 275, ISBN: 3-527-40532-1.
- [6] A.A. Bokov, *Ferroelectrics* **131** 49 (1992); A.A. Bokov, L.A. Shpak and I.P. Raevsky, *J. Phys. Chem. Sol.* **54** 495 (1993).
- [7] C. Stock, R.J. Birgeneau, S. Wakimoto, J.S. Gardner, W. Chen, Z.-G. Ye and G. Shirane, *Phys. Rev. B* **69** 094104 (2004).
- [8] G. Xu, Z. Zhong, Y. Bing, Z.-G. Ye, C. Stock and G. Shirane, *Phys. Rev. B* **70** 064107 (2004).
- [9] C. Conlon, H. Luo, D. Viehland, J.F. Li, T. Whan, J.H. Fox, C. Stock and G. Shirane, *Phys. Rev. B* **70** 172204 (2004).
- [10] G. Xu, H. Hiraka, G. Shirane and K. Ohwada, *Appl. Phys. Lett.* **84**(20) 3975 (2004).
- [11] V. Westphal, W. Kleemann and M.D. Glinchuk, *Phys. Rev. Lett.* **68** 847 (1992).
- [12] H. Quian and L.A. Bursill, *Int. J. Mod. Phys.* **10** 2027 (1996).
- [13] R. Fisch, *Phys. Rev. B* **67** 094110-1 (2003).
- [14] C.G.F. Stenger, F.L. Scholten and A.J. Burggraaf, *Solid State Comm.* **32** 989 (1979); See also: C.G.F. Stenger and A.J. Burggraaf, *Phys. Status Solidi* **61** 275 (1980), C.G.F. Stenger and A.J. Burggraaf, *Phys. Status Solidi* **61** 653 (1980).
- [15] C. Perrin, N. Menguy, O. Bidault, C.Y. Zahara, A.M. Zahara, C. Caranini, B. Hilczler and A. Stepanov, *J. Phys. Condens. Matter* **13** 10231 (2001).
- [16] C. Perrin, N. Menguy, E. Suard, Ch. Muller, C. Caranoni and A. Stepanov, *J. Phys. Cond. Matter* **12** 7523 (2000).
- [17] F. Chu, N. Setter and A.K. Tagantsev, *J. Appl. Phys.* **74**(8) 5129 (1993).
- [18] I.M. Reaney, J. Petzelt, V.V. Votisekhovskii, F. Chu and N. Setter, *J. Appl. Phys.* **76**(4) 2086 (1994).
- [19] F. Chu, I.M. Reaney and N. Setter, *J. Appl. Phys.* **77**(4) 1671 (1995).
- [20] L.A. Bursill, J.-L. Peng, H. Qian and N. Setter, *Physica B.* **205** 305 (1995).
- [21] F. Chu, I.M. Reaney and N. Setter, *J. Amer. Ceram. Soc.* **78**(7) 1947 (1995).
- [22] F. Chu, G. Fox and N. Setter, *J. Amer. Ceram. Soc.* **81**(6) 1577 (1998).
- [23] E. Cockayne and B.P. Burton, *Phys. Rev. B* **69** 144116 (2004).
- [24] E.I. Venturini, R.K. Grubbs, G.A. Samara, Y. Bing and Z.-G. Ye, *Phys. Rev. B* (2005) (Submitted).
- [25] G.A. Samara, *Phys. Rev. Lett.* **77** 314 (1996). Also: *J. Appl. Phys.* **84** 2538 (1998).

- [26] G.A. Samara, in *Fundamental Physics of Ferroelectrics 2000*, edited by R.E. Cohen (American Institute of Physics, New York, 2000), p. 344.
- [27] J. Kreisel, B. Dkhil, P. Bouvier and J.-M. Kiat, *Phys. Rev. B* **65** 172101 (2002).
- [28] G.A. Samara, *J. Phys.: Condens. Matter* **15** R367 (2003).
- [29] B. Chaabane, J. Kreisel, B. Dkhil, P. Bouvier and M. Mezouar, *Phys. Rev. Lett.* **90** 257601 (2003).
- [30] M. Szafranski, A. Hilezer and W. Nawrocki, *J. Phys. Condens. Matter* **16** 7025 (2004).
- [31] G.A. Samara, *Phys. Rev.* **151** 378 (1966).
- [32] G.A. Samara, *Phys. Rev. Lett.* **27** 103 (1971).
- [33] G.A. Samara, T. Sakudo and K. Yoshimitsu, *Phys. Rev. Lett.* **35** 1767 (1975).
- [34] J.A. Sanjurjo, E. Lopez-Cruz and G. Burns, *Phys. Rev. B* **28** 7260 (1983).
- [35] M.A. Akbas and P.K. Davies, *J. Am. Ceram. Soc.* **80**(11) 2933 (1997).
- [36] M.A. Akbas and P.K. Davies, *J. Am. Ceram. Soc.* **81**(11) 1061 (1998).
- [37] M.A. Akbas and P.K. Davies, *J. Am. Ceram. Soc.* **81**(11) 2205 (1998).
- [38] M.A. Akbas and P.K. Davies, *J. Am. Ceram. Soc.* **83**(1) 119 (2000).
- [39] H.B. Krause, J.M. Cowley and J. Wheatley, *Acta. Cryst.* **A35** 1015 (1979).
- [40] E. Husson, M. Chubb and A. Morell, *Mat. Res. Bull.* **V23** 357 (1988).
- [41] E. Husson, L. Abello and A. Morell, *Mat. Res. Bull.* **V25** 539 (1990).
- [42] A.D. Hilton, D.J. Barber, C.A. Randall and T.R. ShROUT, *J. Mater. Sci.* **25** 3461 (1990).
- [43] H.D. Rosenfeld and T. Egami, *Ferroelectrics* **158** 351 (1994).
- [44] T. Mishima, H. Fujioka, S. Nagakari, K. Kamigaki and S. Nambu, *Jpn. J. Appl. Phys.* **36** 6141 (1997).
- [45] H.Z. Jin, J. Zhu, S. Miao, X.W. Zhang and Z.Y. Cheng, *J. App. Phys.* **89**(9) 5048 (2001).
- [46] S. Miao, J. Zhu, X. Shang and Z.-Y. Cheng, *Phys. Rev. B* **65** 052101 (2001).
- [47] C.A. Randall and A.S. Bhalla, *Jpn. J. Appl. Phys.* **29**(2) 327 (1990). Also, C.A. Randall, A.S. Bhalla, T.R. ShROUT and L.E. Cross, *J. Mater. Res.* **5** 829 (1990).
- [48] G. Burns and F.H. Dacol, *Solid State Comm.* **48**(10) 853 (1983).
- [49] R. Blinc, V.V. Laguta and B. Zalar, *Phys. Rev. Lett.* **91**(24) 247601-1 (2003).
- [50] P. Bonneau, P. Garnier, G. Calvarin, E. Husson, J.R. Gavarrri, A.W. Hewat and A. Morell, *J. Solid. State Chem.* **91** 350 (1991).
- [51] J. Zhao, A.E. Glazounov, Q.M. Zhang and B. Toby, *Appl. Phys. Lett.* **73**(9) 1048 (1998).
- [52] B. Dkhil, J.M. Kiat, G. Calvarin, G. Baldinozzi, S.B. Vakhrushev and E. Suard, *Phys. Rev. B* **65** 024104 (2001).
- [53] A. Naberezhnov, S. Vakhrushev, B. Dorner, D. Strauch and H. Moudden, *Eur. Phys. J. B* **11** 13 (1999).
- [54] K. Hirota, S.G. Ye, S. Wakimoto, P.M. Gehring and G. Shirane, *Phys. Rev. B* **65** 104105 (2002).
- [55] H. Hiraka, S.-H. Lee, P.M. Gehring, G.Y. Xu and G. Shirane, <http://arxiv.org/pdf/cond-mat/0403544>
- [56] G.Y. Xu, G. Shirane, J.R.D. Copley and P.M. Gehring, *Phys. Rev. B* **69** 064112 (2004).
- [57] I.K. Jeong, T.W. Darling, J.K. Lee, Th. Proffen, H. Heffner, J.S. Park, K.S. Hong, W. Dmowski and T. Egami, *Phys. Rev. Lett.* **94** 147602 (2005).
- [58] J. Chen, H. Chan and M. Harmer, *J. Am. Ceram. Soc.* **72**(4) 593 (1989).
- [59] D. La-Orauttapong, J. Toulouse, Z.-G. Lee, W. Chen, R. Irwin and J.L. Robertson, *Phys. Rev. B* **65** 144101 (2002).
- [60] D. La-Orauttapong, O. Svitelskiy and J. Toulouse, <http://arxiv.org/pdf/cond-mat/0303004>
- [61] D. La-Orauttapong, J. Toulouse, Z.-G. Lee, W. Chen, R. Irwin and J.L. Robertson, *Phys. Rev. B* **67** 134110 (2003).
- [62] G. Calvarin, E. Husson and S.G. Ye, *Ferroelectrics* **165** 349 (1995).
- [63] T.R. Welberry, M.J. Gutmann, H. Woo, D.J. Goossens, G.Y. Xu, C. Stock, W. Chen and Z.-G. Ye, *J. Appl. Cryst.* **38**(4) 639 (2005).
- [64] G.Y. Xu, Z. Zhong, H. Hiraka and G. Shirane, *Phys. Rev. B* **70** 174109 (2004).
- [65] N. Setter and L.E. Cross, *J. Appl. Phys.* **51** 4356 (1980); See also: *Phys. Status. Solidi* **61** K71 (1980), and *J. Matter Sci.* **15** 2478 (1980).
- [66] C.A. Randall, D.J. Barber, R.W. Whatmore and P. Groves, *J. Mater. Sci.* **21** 4456 (1986).
- [67] C.A. Randall, S.A. Markgraf, A.S. Bhalla and K.Z. Baba-Kishi, *Phys. Rev. B* **40**(1) 413 (1989).
- [68] K.Z. Baba-Kishi and D.J. Barber, *J. App. Cryst.* **23** 43 (1990).

- [69] K.Z. Baba-Kishi, G. Cressey and R.J. Cernik, *J. Appl. Cryst.* **25** 477 (1992).
- [70] P. Lampin, N. Menguy and C. Caranoni, *Phil. Mag. Lett.* **B 72**(4) 215 (1995).
- [71] J.R. Giniewicz, A.S. Bhalla and L.E. Cross, *Ferroelectrics* **211** 281 (1998).
- [72] B.P. Burton and E. Cockayne, *Phys. Rev. B* **60** R12542 (1999).
- [73] B.P. Burton, *Modeling Simul. Matter Sci. Eng.* **8** 211 (2000).
- [74] B.P. Burton and E. Cockayne, *J. Phys. Chem. Solids* **61** 327 (2000).
- [75] B.P. Burton and E. Cockayne, *Ferroelectrics* **270** 173 (2002).
- [76] M. Wensell and H. Krakauer, *J. Phys. Chem. Solids* **61** 309 (2000).
- [77] S.A. Prosandeev, E. Cockayne and B.P. Burton, in *Fundamental Physics of Ferroelectrics* (A.I.P. Conf. Proc.), edited by P.K. Davies and D.J. Singh (Volume 677, 2003), p. 146.
- [78] E. Cockayne, unpublished (2005).
- [79] Z. Wu and H. Krakauer, *Phys. Rev.* **63** 184113 (2001).
- [80] B.P. Burton, U.V. Waghmare and E. Cockayne, *TMS Letters* **1**(2) 29 (2004).
- [81] J. Ravez and A. Simon, *Eur. J. Solid State Inorg. Chem.* **34** 1199 (1997).
- [82] A. Dixit, S.B. Majumder, A. Savvinov, R.S. Katiyar, R. Guo and A.S. Bhalla, *Matter. Lett.* **56** 933 (2002).
- [83] Y. Hotta, G.W.J. Hassink, T. Kawai and H. Tabata, *Japan. J. Appl. Phys.* **42** 5908 (2003).
- [84] J. Zhai, X. Yao, J. Shen, L. Zhang and H. Chen, *J. Phys. D Appl. Phys.* **37** 748 (2004).
- [85] J. Kreisel, P. Bouvier, M. Maglione, R. Dkhil and A. Simon, *Phys. Rev. B* **69** 092104 (2004).
- [86] V.V. Bhat, A.M. Umarji, V.B. Shenoy and U.V. Waghmare, *Phys. Rev. B* **72** 014104 (2005).
- [86a] I. Grinberg and A. Rappe, *Phys. Rev. B* **70** 220101(R) (2004).
- [87] N. Takesue, Y. Fujii, M. Ichihara and H. Chen, *Phys. Rev. Lett.* **82** 3709 (1999).
- [88] N. Takesue, Y. Fujii, M. Ichihara, H. Chen, S. Tatemori and J. Hatano, *J. Phys. Cond. Matter* **11** 8301 (1999).
- [89] N. Takesue, Y. Fujii and H. You, *Phys. Rev. B* **64** 184112-1 (2001).
- [90] S.N. Gvasaliya, B. Roessli and S.G. Lushnikov, *Europhys. Lett.* **63** 303 (2003).
- [91] S.N. Gvasaliya, S.G. Lushnikov and B. Roessli, *Phys. Rev. B* **69** 092105 (2004).
- [92] S. Vakhrushhev, B. Kvyatkovsky, A. Naberezhnov, W. Okuneva and B. Toperverg, *Ferroelectrics* **90** 173 (1989).
- [93] V. Gosula, A. Tkachuk, K. Chung and H. Chen, *J. Phys. Chem. Solids* **61**(2) 221 (2000).
- [94] H. You, *J. Phys. Chem. Solids* **61**(2) 215 (2000).
- [95] B. Chaabane, J. Kreisel, B. Dkhil, P. Bouvier and M. Mezouar, *Phys. Rev. Lett.* **90** 257601 (2003).
- [96] U.V. Waghmare, E. Cockayne and B.P. Burton, *Ferroelectrics* **291** 187 (2003).
- [97] K.M. Rabe and U.V. Waghmare, *Phys. Rev. B* **52** 13236 (1995).
- [98] K.M. Rabe and U.V. Waghmare, *Ferroelectrics* **194** 119 (1996).
- [99] U.V. Waghmare and K.M. Rabe, *Phys. Rev. B* **55** 6161 (1997).
- [100] W. Zhong, D. Vanderbilt and K.M. Rabe, *Phys. Rev. B* **52** 6301 (1995).
- [101] P.K. Davies, L. Farver, M. Valant and M.A. Akbas, *J. Am. Ceram. Soc.* **85** 2319 (2002).
- [102] R. Hemphill, L. Bellaiche, A. Garcia and D. Vanderbilt, *Appl. Phys. Lett.* **77** 3642 (2000).
- [103] E. Cockayne, B.P. Burton and L. Bellaiche, in *Fundamental Physics of Ferroelectrics 2001* (AIP Conf. Proc.), edited by H. Krakauer (Volume 532, 2001), p. 191. Also E. Cockayne (Unpublished results).
- [104] J. Íñiguez and L. Bellaiche, *Phys. Rev. Lett.* **87** 095503 (2001).
- [105] A.M. George and L. Bellaiche, in *Fundamental Physics of Ferroelectrics 2001: 11th Williamsburg Ferroelectric Workshop*, edited by H. Krakauer (AIP, Melville, New York, 2001), p. 62.
- [106] A.M. George and L. Bellaiche, *Phys. Rev. B. (Rapid Comm.)* **64** 060102 (2001).
- [107] A.M. George and L. Bellaiche, in *First-Principles Calculations for Ferroelectrics: Fifth Williamsburg Workshop*, edited by R.E. Cohen (AIP, Woodbury, New York, 1998), p. 11.

- [108] A.M. George and L. Bellaiche, in *Proceedings of the 2000 Aspen Winter Conference on Fundamental Physics of Ferroelectrics*, edited by R.E. Cohen (AIP, Woodbury, New York, 2000), p. 79.
- [109] L. Bellaiche, A. Garcia and D. Vanderbilt, *Phys. Rev. Lett.* **84** 5427 (2000).
- [110] L. Bellaiche, A. Garcia and D. Vanderbilt, *Phys. Rev. B (Rapid Comm.)* **64** 060103 (2001).
- [111] L. Bellaiche, A. Garcia and D. Vanderbilt, *Ferroelectrics* **266** 41 (2002).
- [112] A. Sani, B. Noheda, I.A. Kornev, L. Bellaiche, P. Bouvier and J. Kreisel, *Phys. Rev. B (Rapid Comm.)* **69** 020105 (2004).
- [113] K.S. Knight and K.Z. Baba-Kishi, *Ferroelectrics* **173** 341 (1995).
- [114] V.V. Laguta, M.D. Glinchuk, I.P. Bykov, R. Blinc and B. Zalar, *Phys. Rev. B* **69** 054103 (2004).
- [115] R. Pirc and R. Blinc, *Phys. Rev. B* **60**(19) 13470 (1999).
- [116] B.P. Burton, E. Cockayne and U.V. Waghmare, *Phys. Rev. B* **72** 064113 (2005).
- [117] R.E. Cohen, *Nature (London)* **358** 137 (1992). Also, R.E. Cohen and H. Krakauer, *Ferroelectrics* **136**(1–4) 65 (1992).
- [118] G. Saghi-Szabo, R.E. Cohen and H. Krakauer, *Phys. Rev. Lett.* **80** 4321 (1998).
- [119] M. Fornari and D. Singh, *Phys. Rev. B* **63** 092101 (2001).
- [120] N. Yasuda, H. Ohwa and T. Mizuno, *Appl. Phys. Lett.* **68**(24) 3404 (1996).
- [121] K. Nomura, T. Shingai, N. Yasuda, H. Ohwa and H. Terauchi, *J. Phys. Soc. Japan* **68**(3) 8666 (1999).
- [122] Y. Yoneda, N. Matsumoto, H. Terauchi and N. Yasuda, *J. Phys. Cond. Matter* **15** 467 (2003).
- [123] J. Íñiguez, J.B. Neaton and D. Vanderbilt, in *Fundamental Physics of Ferroelectrics* (A.I.P. Conf. Proc.), edited by P.K. Davies and D.J. Singh (Volume 677, 2002), p.146.
- [124] R. Blinc, J. Dolinsek, A. Gregorovic, B. Zalar, C. Filipic, Z. Kutnjak, A. Levstik and R. Pirc, *Phys. Rev. Lett.* **83** 424 (1999).
- [125] I. Imry and S.L. Ma, *Phys. Rev. Lett.* **35** 1399 (1975).
- [126] R.D. Shannon, *Acta. Cryst.* **A32** 751 (1976). <http://abulafia.mt.ic.ac.uk/shannon/>